PROCEEDINGS OF THE SIXTEENTH LUNAR AND PLANETARY SCIENCE CONFERENCE, PART 2
JOURNAL OF GEOPHYSICAL RESEARCH, VOL. 91, NO. B4, PAGES D277–D303, MARCH 30, 1986

Apollo 16 Regolith Breccias: Characterization and Evidence for Early Formation in the Mega-Regolith

D. S. McKay[1], D. D. Bogard,[1] R. V. Morris[1], R. L. Korotev[2], P. Johnson[3], and S. J. Wentworth[4]

All of the Apollo 16 regolith breccias (18 specimens) have been characterized in terms of their petrography, grain-size distribution, porosity, major and trace element composition, noble gas contents, and ferromagnetic resonance properties. These breccias vary significantly with respect to their density and porosity, with the more dense breccias showing significant shock damage. The regolith breccias resemble the soils in grain-size distribution and in the relative proportions of major petrological components, except agglutinates. Many of the breccias are compositionally different from the Apollo 16 soils in that they lack an important mafic component present in the soils. Although some groupings occur, the petrologic and chemical compositions of the regolith breccias do not correlate with the station location of the samples. All but one of the breccias show some evidence of irradiation at the lunar surface (solar gases, measurable FMR, agglutinates), and analyses made on grain-size separates from two disaggregated breccias indicate that this irradiation occurred before compaction when the breccia material was finely disseminated on the surface. However, the concentrations of surface irradiation parameters (solar gases, FMR, agglutinates) for most breccias are far less than seen in any lunar soils or in regolith breccias from other Apollo missions. Several breccias also contain unusually high trapped $^{40}Ar/^{36}Ar$ ratios of ~8–12 and a significant fission Xe component in excess of that expected from in situ production. These observations suggest that the surface irradiation of these breccias occurred as early as 4×10^9 years ago. We conclude that most of the Apollo 16 regolith breccias were not formed from any known Apollo 16 soil. They appear to be well-comminuted material that contains ancient regolith developed during the late stage heavy bombardment of the moon when large impacts were much more common relative to small impacts so that regoliths did not have time to significantly mature before being diluted by fresh ejecta and buried. This ancient megaregolith is significantly different from more recent lunar regolith but may be similar to asteroidal regoliths from which some brecciated meteorites have formed.

Introduction

Regolith breccias are fragmental breccias containing some identifiable regolith component such as glass spherules or agglutinates [*Stöffler et al.*, 1979]. They are normally thought of as the indurated equivalent of ordinary lunar soil, although for reasons to be discussed in this paper we believe that this explanation is too simple. We have been studying a suite of regolith breccias from both the Apollo 15 and 16 sites including nearly all of the identified regolith breccia samples larger than 1 cm (except for some rake samples). A comparison of regolith breccias from these two sites should reveal differences between regolith breccias made mainly from highland material and regolith breccias containing major amounts of mare material. Apollo 15 and 16 regolith breccias may also represent different time periods in lunar history. Data on Apollo 15 regolith breccias will be presented elsewhere. Although many of the individual breccias have been studied and analyzed by various techniques, this is the first attempt to study the entire suite of regolith breccias using a multidisciplinary approach that includes petrography, texture analysis, ferromagnetic resonance analysis (FMR), rare gas analysis, and chemical analysis by instrumental neutron activation (INAA). The combination of these techniques, previously used extensively on lunar soils, allows for a detailed analysis of the maturity of lunar breccias, or more precisely, the maturity of the regolith material from which they were made. The maturity of these breccias has not been previously determined in any systematic way.

An important feature of regolith breccias is that they contain samples of regolith that were closed to further regolith processing at the time they were assembled into rocks. The regolith preserved in these breccias, if not too modified by the breccia-forming event, is essentially a snapshot of lunar (and solar system) conditions at the time the breccia was formed. We believe that this enormously important potential of regolith breccias has been nearly overlooked in the study of lunar samples and that regolith breccias may ultimately provide a key to understanding events and conditions on the lunar surface, properties of the ancient sun, and properties of the meteoroid complex back through geologic time. The problem then, is to analyze these regolith breccias, determine when they were formed and the age of the regolith material within them, and determine what their properties might reveal about lunar and solar system history. While it is very difficult to positively date the breccia-forming event, some indirect evidence for the age of regolith breccias can be deduced from the rare gas data and, as discussed later in this paper, some of the Apollo 16 breccias may be very ancient and may preserve the oldest samples of regolith yet found on the moon.

Descriptions of regolith breccias from Apollo 16 are found in the Apollo 16 catalog [*Ryder and Norman*, 1980] and in the Regolith Breccia Workbook [*Fruland*, 1983]. Both of these compilations include extensive references to the earlier work on these breccias that we will not repeat here. Returned regolith breccias are not evenly distributed among the Apollo 16 stations. More than half come from the vicinity of the LM on the Cayley Plains (Station 1 and 10). None come from Station 4 on Stone Mountain or from the rim of North Ray crater at Station 11,

[1]Solar System Exploration Division, NASA Johnson Space Center
[2]Department of Earth and Planetary Sciences and the McDonnell Center for the Space Sciences, Washington University
[3]Northrop Services, Incorporated
[4]Lockheed/LEMSCO

Paper number 5B7052.

TABLE 1. Porosity, Regolith Components, and Shock Features for Apollo 16 Regolith Breccias

Sample	Intergranular Fracture Porosity	Intergranular Fracture Porosity*	Agglutinates†	Spheres	Shock Features‡
60016	subporous	low	rare	rare	rare
60019	compact	intermediate	none	rare	common
60255	compact	high	rare	rare	common
60275	compact	intermediate	none	rare	common
61135	subporous	low	rare	rare	minor
61175	porous	low	minor	rare	rare
61195	compact	intermediate	rare	rare	common
61295	subporous	low	rare	rare	rare
61516	subporous	low	minor	rare	rare
61525	subcompact	intermediate	rare	rare	common
61536	subcompact	intermediate	rare	rare	common
63507	porous	low	common	rare	rare
63588	subporous	low	rare	rare	minor
63595	subporous	low	none	rare	minor
65095	subporous	low	rare	rare	minor
65715	subporous	low	rare	rare	minor
66035	subporous	low	rare	rare	minor
66036	subporous	low	rare	rare	rare
66075	subporous	low	rare	rare	minor
	Fragmental Breccias (No Regolith Component)				
60075	compact	low	none	none	minor
63577	compact	low	none	none	minor
67016	porous	low	none	none	minor
67035	subporous	low	none	none	minor
67455	subporous	low	none	none	rare

All Apollo 16 regolith breccias are shown, plus some fragmental breccias from Apollo 16 that are not regolith breccias. Porosity classification is based on optical microscope examination in reflected light.

*Includes fractures and vesicularity.

†Rare means questionable to 1 vol %, minor means 1% to 5%, and common means more than 5%.

‡Shock features include fracturing of grains, intergranular fracturing, glass veins and matrix, resorption of clasts in glassy matrix, and undulatory extinction.

although *Stöffler et al.* [1981] identify one 3-g regolith breccia sample among the 102 rake samples they studied from Station 11. Whether this distribution pattern reflects actual field abundances or whether it is a sampling artifact remains uncertain.

TEXTURES AND POROSITY

The Apollo 16 regolith breccias range from very tough and coherent rocks to rocks that are very friable and clod-like. *Chao et al.* [1971] was the first to distinguish porous and nonporous regolith breccias. We have used this textural property as the basis for a simple classification system in which the intergranular porosity in thin sections was estimated in reflected light (Table 1). This table also includes an estimate of porosity present in fractures and vesicles, an estimate of the agglutinate and glass sphere abundance, and an estimate of the abundance of obvious shock features, including undulatory extinction, vein glass, and planar features in minerals. The porosity-based classification is also suitable for fragmental breccias that do not contain identifiable regolith components, and several of these breccias are included in Table 1 for comparison.

As an independent check of our porosity estimates, we have measured densities using plastic rock models made from the original rocks and have calculated porosities for a number of regolith breccias [*Wentworth and McKay*, 1984]. In this technique, porosities were calculated for breccias that had the necessary compositional data and available plastic models by comparing measured bulk densities to calculated intrinsic densities. The bulk densities were measured by dividing original sample weights by volumes obtained by using Archimedes' principle on plastic models of the samples. The plastic models were made during original sample processing from molds formed by carefully wrapping the rocks in aluminum foil. We measured the volume of each model 10 times and the mean value was used in the calculations. Intrinsic densities were calculated from CIPW norms of previously published chemical analyses. Typical mineral densities were assumed for normative minerals. The normative calculations do not make allowance for the presence of glass in the regolith breccias, creating additional uncertainty in the calculations. Porosities were also independently estimated from Scanning Electron Microscope (SEM) modes by counting pore spaces in thin sections of several of the breccias during modal analyses of the <20-μm fractions (approximately 800 points per section). These data are presented in Table 2 along with previously published density determinations.

A strong correlation exists between porosity and visible shock features; only subcompact and compact breccias show clear indications of shock damage (Table 1). In porous and subporous breccias, visible shock damage is rare. Porosity present as fractures in grains or matrix is common only in compact and subcompact breccias. In compact breccias, such porosity dominates the intergranular porosity. Agglutinates or sphere are present in all of the regolith breccias but are common only in the porous ones. This may be partly an artifact, however; the process that makes regolith breccias compact also makes agglutinates difficult to identify in thin section. Spheres, however, are distinctive in both porous and compact breccias.

Comparison of our measured densities with previously published values is generally good (Table 2), although our densities tend to be lower than published values. Where significant differences exist we favor our value because we used the rock model made from the entire rock rather than a small chip as was used on some of the previous density determinations. The comparison between our calculated porosities and the independently estimated porosities based on SEM modes is also good.

A qualitative correlation exists between the measured densities in Table 2 and the petrographic porosity determined from polished thin sections: The compact breccias have the highest bulk densities. This correlation adds support to the validity of the petrographic classification and is evidence that the textures observed in thin section are reasonably representative of the entire rock. The measured bulk density values presented in Table 2 range from 1.92 to 2.31 g/cm^3. These values can be compared with bulk densities for Apollo 16 soil determined for the drive tubes [*Mitchell et al.*, 1972] that range from 1.40 to 1.80 g/cm^3. Clearly, the density of even the most porous of the Apollo 16 regolith breccias is greater than that of the most compressed unconsolidated soil found at depth in the drive tubes. A similar comparison can be made for the porosities. The range of measured and calculated porosities for regolith breccias as shown in Table 2 is from 20.6% to 31.9%. Porosities of soil deduced from penetrometer and footprint data [*Mitchell et al.*, 1972] range from 32% to 55%. Again, there is essentially no overlap. The porosities measured for chondrites are nearly all lower than 20% [*Fujii et al.*, 1981; *Hamano and Yomogida*, 1982; *Yomogida and Matsui*, 1982]. This observation may have some significance in terms of meteorites reaching the surface of the earth. Perhaps meteorites of higher porosity exist, comparable to the porosities

TABLE 2. Density and Porosity for Apollo 16 Regolith Breccias

Sample	Intergranular Porosity (Petrographic)	Bulk Density (gm/cm^3)	Intrinsic Density (gm/cm^3)	Previous Density Values (gm/cm^3)	Calculated Porosity (percent)	Porosity from SEM Modes (percent)
60016	subporous	2.11	2.89		27.0	27.5
60019	compact	2.23	2.91		23.4	
60255	compact	2.31	2.91		20.6	
60275	compact	2.26	2.92		22.6	
61135	subporous	1.92		2.0–2.1*		
61175	porous	1.96	2.88	2.25†	31.9	
61195	compact	2.42	2.90	2.5–2.6*	16.6	
65095	subporous	1.94		2.5–2.6*		
66035	subporous	2.05	2.84	2.2–2.3*	27.8	25.9
66075	subporous	2.11	2.89	2.4–2.5*	27.0	23.6

Included are measured bulk density, intrinsic density calculated from normative mineralogy, calculated porosity, and porosity measured with the Scanning Electron Microscope (SEM) for selected breccias.
Sources for previously published density values:
*Talwani et al. [1973].
‡Mizutani et al. [1974].

of Apollo 16 regolith breccias, but they do not normally survive entry through the earth's atmosphere. It would be profitable to compare our lunar regolith breccia data and the existing meteorite data to the porosities of the recently identified lunar meteorites found in Antarctica.

Porosities of regolith breccias are determined by the breccia-forming event whether by shock compaction, thermal sintering, or some combination of the two processes. Porosities might be reduced by subsequent shock or thermal events. More compact regolith breccias are likely to have experienced a more energetic subsequent processing compared to porous breccias. Consequently, the porosity may be correlated with other properties of the breccias, including rare gas retention, volatile redistribution or loss, possible resetting of some isotopic systems, and possible annealing of particle tracks. For example, partial fading of particle tracks observed in compact breccia 60255 indicates that this breccia may have been thermally annealed to between 700° and 800°C [*MacDougall et al.*, 1972].

PETROLOGY

We have examined and described polished thin sections of all of the identified regolith breccias, and we have made modal analyses of all of the porous and subporous breccias. We were not able to accurately determine original clast and grain boundaries in compact and subcompact breccias and therefore have not included them in the modal analysis tables. Table 3 presents data on the larger clasts (>500 μm) in the analyzed breccias. This table also contains the percentage of each breccia consisting of <20-μm matrix and pore space. Table 4 and Figure 1 present modal data on the size range from 20 to 500 μm. Terminology is defined in Appendix 1.

A number of features of these tables should be noted. As is true for soils, lithic fragments make up the bulk of all particles larger than 500 μm (Table 3). Major classes of lithic fragments include anorthosites, norites and troctolites, subophitic and intergranular varieties of impact melt rocks, and poikilitic melt rocks. Some breccias are dominated by one of these types: 66035, 66036, and 65715 contain mainly anorthosites in this coarser size fraction while 61516, 65095, and 66075 contain mainly subophitic melt rocks with minor amounts of anorthosite. However, in some of the thin sections the point-count abundance of large grains is dominated by a small number of especially large lithic clasts. Furthermore, in smaller thin sections the total number of grains larger than 500 μm is small. The percentages therefore are subject to considerable uncertainty due to sampling problems and only general trends are indicated by the percentage values. The coarser mineral fragments are almost entirely plagioclase; olivines and pyroxenes larger than 500 μm are nearly nonexistent in the sections examined. The only other coarse-grained components are ropy and vitrophyric glass particles, are present in abundances of up to 29% in breccia 63588.

The data on the 20–500-μm size fraction are more representative (Table 4). For most thin sections, approximately 800 points were identified and tabulated, of which at least 300 were in the 20–500-μm size fraction. For comparison, a section from the set of continuous thin sections of drive tube 60010 was also point-counted. This core soil is reasonably representative of submature soils at the Apollo 16 site. The major component in all samples consists of monomineralic plagioclase fragments that make up about half of this size fraction for many of the regolith breccias. Olivine is the next most abundant mineral, followed by pyroxene. Total mineral fragment abundances range from a low of 22% for 63507 to a high a 68% for 66075. Crystalline lithics including anorthosite, norite, and troctolite types ranged from 5% to 20% of fragments. With one exception (66975), all the regolith breccias contain significantly more of these rock types than the core soil (60010,6037). Breccia fragments are almost entirely of the melt matrix and granulitic varieties; fragments of regolith breccias and fragmental breccias are extremely rare. This observation suggests that the regolith breccias at the Apollo 16 site are not, in general, multigenerational regolith breccias.

The ratio of the crystalline lithic suite (mainly anorthosites with lesser amounts of norite and troctolite fragments) to the melt matrix breccia suite (mainly poikilitic, subophitic, and intergranular textures) varies considerably from breccia to breccia. In Figure 2, the percentage of lithic fragments that are anorthosites, norites, and troctolites (ANT) in the combined group, which includes these lithic types plus the melt matrix lithic types, is plotted against the FeO content of the regolith breccias (discussed in a subsequent section). Breccia 63507 has been omitted from this graph because the anomalously high meteoritic contribution to this breccia has significantly affected the FeO content (see subsequent section on breccia chemistry). The least squares fit to the remaining regolith breccias is shown

on Figure 2 and has a correlation R of 0.80. If this relationship can be interpreted as a mixing line, it suggests that chemical differences among the regolith breccias may be mainly a result of variations in the ratios of these rock types. Extrapolation of the least squares fit in Figure 2 to 0% ANT suite gives an FeO content of 5.9% for the melt matrix suite. This value is typical for many of the basaltic impact melt rocks described in the Apollo 16 catalog [*Ryder and Norman,* 1980]. These rocks are petrologically similar to many of the particles in our melt matrix category. Extrapolation of the line in Figure 2 to 100% ANT suite gives an FeO content of 1.88% for this suite. This value is too high for Apollo 16 anorthosites, which generally contain less than 0.5% FeO. However, it is appropriate for a mixture of anorthosite and anorthositic norite.

While found at all stations, mafic melt matrix breccias (also called basaltic impact melt rocks) are more common in the central and southern parts of the site in areas usually mapped as Cayley [*Stöffler et al.*, 1981; *James*, 1981]. Anorthosites and granulitic norites and troctolites are also found at all stations. They are common at Station 11 and 13 where they are presumed to be clasts derived from feldspathic fragmental breccias [*James*, 1981]. *Minkin et al.* [1977] found that 70% of the lithic clasts (>40 μm) in feldspathic fragmental breccia 67455 were cataclastic anorthosite or granulitic breccias; the remainder were melt matrix breccias and other types. If these numbers are typical for Station 11, then, compared to stations in the central and

TABLE 3. Optical Modes of >500-μm Particle Types in Apollo 16 Regolith Breccias

Sample	60016	61135	61175	61295	61516	63507	63588
Section Number	171 and 172	8	108	37	4	14	5
Percent >500 μm	21.3	19.5	14.9	20.1	4.3	7.8	6.2
Percent 20–500 μm	37.0	34.8	34.4	35.6	39.9	41.6	45.7
Percent <20 μm and Pores	41.7	45.8	50.7	44.4	55.8	50.6	48.1
Percent Total	100.0	100.0	100.0	100.0	100.0	100.0	100.0
Optical Mode: >500 μm (Normalized)							
Monomineralic Fragments							
Plagioclase	14.6	4.2	2.3	1.8	15.4	7.0	0.0
Olivine	0.0	0.0	0.0	0.0	0.0	0.0	0.0
Pyroxene	0.0	0.0	0.0	0.6	0.0	0.0	0.0
Ilmenite	0.0	0.0	0.0	0.0	0.0	0.0	0.0
Spinel	0.0	0.0	0.0	0.0	0.0	0.0	0.0
Troilite	0.0	0.0	0.0	0.0	0.0	0.0	0.0
Metal	0.0	0.0	0.0	0.0	0.0	0.0	0.0
SiO_2	0.0	0.0	0.0	0.0	0.0	0.0	0.0
(Subtotal)	(14.6)	(4.2)	(2.3)	(2.4)	(15.4)	(7.0)	(0.0)
Crystalline Lithics							
Anorthosite	5.5	32.1	17.7	17.2	0.0	8.8	9.8
Norite-Troctolite	11.8	1.2	6.9	4.7	0.0	5.3	22.0
Mare Basalt	0.0	0.0	0.0	0.0	0.0	0.0	0.0
KREEP Basalt	0.0	11.3	0.0	1.2	0.0	0.0	0.0
Other/Indet	0.0	0.0	0.0	0.0	0.0	0.0	0.0
(Subtotal)	(17.3)	(44.6)	(24.6)	(23.1)	(0.0)	(14.0)	(31.7)
Breccias							
Regolith Porous	0.0	0.0	0.0	10.7	0.0	0.0	0.0
Regolith Compact	0.0	0.0	0.0	0.0	0.0	0.0	0.0
Vitric Porous	0.0	0.0	0.0	0.0	0.0	0.0	0.0
Vitric Compact	5.5	10.1	3.1	3.6	0.0	0.0	19.5
Fragmental Porous	0.0	0.0	56.9	3.0	0.0	0.0	19.5
Fragmental Compact	0.0	0.0	0.8	0.0	0.0	0.0	0.0
(Subtotal)	(5.5)	(10.1)	(60.8)	(17.2)	(0.0)	(0.0)	(39.0)

TABLE 3. (continued)

Sample	60016	61135	61175	61295	61516	63507	63588
Section Number	171 and 172	8	108	37	4	14	5
Crystalline/Melt Matrix							
Poik., Eq. Plag.	23.6	17.3	0.0	1.8	0.0	24.6	0.0
Poik., Acic. Plag.	0.0	0.0	0.0	0.0	0.0	0.0	0.0
Variolitic	0.0	0.0	0.0	3.6	0.0	0.0	0.0
Subophitic	31.8	2.4	3.1	34.3	84.6	8.8	0.0
Intergranular	7.3	20.2	3.9	5.9	0.0	43.9	0.0
Intersertal	0.0	0.0	0.0	3.0	0.0	0.0	0.0
Porphyritic	0.0	0.0	0.0	0.0	0.0	0.0	0.0
Granulitic	0.0	0.0	0.0	3.6	0.0	0.0	0.0
(Subtotal)	(62.7)	(39.9)	(6.9)	(52.1)	(84.6)	(77.2)	(0.0)
Glasses							
Inhomogeneous							
Clastic/Ropy	0.0	0.6	0.0	0.0	0.0	0.0	0.0
Quenched/Vitrophyric	0.0	0.6	2.3	5.3	0.0	1.8	29.3
(Subtotal)	(0.0)	(1.2)	(2.3)	(5.3)	(0.0)	(1.8)	(29.3)
Homogeneous							
Green	0.0	0.0	0.0	0.0	0.0	0.0	0.0
Yellow	0.0	0.0	0.0	0.0	0.0	0.0	0.0
Colorless/Gray	0.0	0.0	3.1	0.0	0.0	0.0	0.0
Black/Orange	0.0	0.0	0.0	0.0	0.0	0.0	0.0
(Subtotal)	(0.0)	(0.0)	(3.1)	(0.0)	(0.0)	(0.0)	(0.0)
Regolith Components							
Spheres	0.0	0.0	0.0	0.0	0.0	0.0	0.0
Agglutinates	0.0	0.0	0.0	0.0	0.0	0.0	0.0
(Subtotal)	(0.0)	(0.0)	(0.0)	(0.0)	(0.0)	(0.0)	(0.0)
Total	100.0	100.0	100.0	100.0	100.0	100.0	100.0
No. of Points >500 μm	110	168	130	169	13	57	41

Sample	63595	65095	65715	66035	66036	66075
Section Number	8	54	5	14	13	70
Percent >500 μm	13.7	40.5	20.4	52.0	2.4	30.6
Percent 20–500μm	43.5	29.5	33.8	23.6	42.7	34.9
Percent <20 μm and Pores	42.8	30.1	45.8	24.4	54.8	34.5
Percent Total	100.0	100.0	100.0	100.0	100.0	100.0
Optical Mode: >500 μm						
Monomineralic Fragments						
Plagioclase	0.0	2.4	10.3	0.0	11.8	3.0
Olivine	0.0	0.0	0.0	0.0	0.0	0.0
Pyroxene	0.0	0.0	0.0	0.0	0.0	0.0
Ilmenite	0.0	0.0	0.0	0.0	0.0	0.0
Spinel	0.0	0.0	0.0	0.0	0.0	0.0
Troilite	0.0	0.0	0.0	0.0	0.0	0.0
Metal	0.0	0.0	0.0	0.0	0.0	0.0
SiO_2	0.0	0.0	0.0	0.0	0.0	0.0
(Subtotal)	(0.0)	(2.4)	(10.3)	(0.0)	(11.8)	(3.0)
Crystalline Lithics						
Anorthosite	24.0	2.2	68.1	94.0	88.2	8.0
Norite-Troctolite	0.0	0.7	0.0	0.0	0.0	2.7
Mare Basalt	0.0	0.0	0.0	0.0	0.0	0.0
KREEP Basalt	0.0	0.0	0.0	0.0	0.0	0.0
Other/Indet	0.0	0.0	0.0	0.0	0.0	0.0
(Subtotal)	(24.0)	(2.9)	(68.1)	(94.0)	(88.2)	(10.6)
Breccias						
Regolith Porous	0.0	0.0	0.0	0.0	0.0	0.0
Regolith Compact	46.0	0.0	0.0	0.0	0.0	0.0
Vitric Porous	0.0	0.0	0.0	0.0	0.0	0.0
Vitric Compact	13.0	2.9	9.2	0.0	0.0	4.2
Fragmental Porous	0.0	0.0	0.0	0.0	0.0	0.0
Fragmental Compact	0.0	0.5	1.6	0.0	0.0	0.0
(Subtotal)	(59.0)	(3.4)	(10.8)	(0.0)	(0.0)	(4.2)

TABLE 3. (continued)

Sample Section Number	63595 8	65095 54	65715 5	66035 14	66036 13	66075 70
Crystalline/Melt Matrix						
Poik., Eq. Plag.	9.0	5.8	0.0	2.8	0.0	5.7
Poik., Acic. Plag.	0.0	0.0	0.0	0.0	0.0	0.0
Variolitic	0.0	0.0	0.0	1.4	0.0	0.0
Subophitic	8.0	82.1	0.0	0.9	0.0	69.2
Intergranular	0.0	1.7	4.3	0.0	0.0	4.6
Intersertal	0.0	0.0	0.0	0.0	0.0	0.8
Porphyritic	0.0	0.0	0.0	0.0	0.0	0.0
Granulitic	0.0	0.0	0.0	0.0	0.0	0.4
(Subtotal)	(17.0)	(89.6)	(4.3)	(5.1)	(0.0)	(80.6)
Glasses						
Inhomogeneous						
Clastic/Ropy	0.0	0.0	0.0	0.0	0.0	0.0
Quenched/ Vitrophyric	0.0	1.7	6.5	0.9	0.0	1.5
(Subtotal)	(0.0)	(1.7)	(6.5)	(0.9)	(0.0)	(1.5)
Homogeneous						
Green	0.0	0.0	0.0	0.0	0.0	0.0
Yellow	0.0	0.0	0.0	0.0	0.0	0.0
Colorless/Gray	0.0	0.0	0.0	0.0	0.0	0.0
Black/Orange	0.0	0.0	0.0	0.0	0.0	0.0
(Subtotal)	(0.0)	(0.0)	(0.0)	(0.0)	(0.0)	(0.0)
Regolith Components						
Spheres	0.0	0.0	0.0	0.0	0.0	0.0
Agglutinates	0.0	0.0	0.0	0.0	0.0	0.0
(Subtotal)	(0.0)	(0.0)	(0.0)	(0.0)	(0.0)	(0.0)
Total	100.0	100.0	100.0	100.0	100.0	100.0
No. of Points >500 μm	100	413	185	207	17	263

These data were acquired by a volumetric point count, and the values may be dominated by one or two large clasts. In particular, in 60016, three clasts dominate the values; in 61516, one lage subophitic clast dominates the point count; in 65095, two large subophitic clasts dominate; in 66035, about half of the available section is one large anorthosite clast; in 66075, one large subophitic clast cominates. Consequently, even though the entire thin section was analyzed in each case, because of the sampling problems, modal percentages should be used with caution and only give indication of the large clast population for the thin sections used. Petrographic descriptions of the classifications used are given in Appendix 1.

southern part of the site, this station is relatively enriched in crystalline lithics.

If the crystalline lithic suite is more characteristic of Descartes material and the melt matrix breccias are more characteristic of Cayley material, then the ratios in Figure 2 represent affinities of the regolith breccias to Descartes and Cayley. These affinities are not simply related to the site where the breccias were found, however. The most Cayley-like regolith breccias based on these ratios are found at Station 5 (65095) and Station 6 (66075), which might be interpreted as good Cayley locations, and the most Descartes-like samples are found at Station 13 (63588 and 63595). However, Station 13 also contained a Cayley-like sample (63507) and Station 5 contained a Descartes-like sample (65715). The sample location for any of these breccias may not reflect the original location at which the breccias were made.

The glass components of the 20–500-μm size fraction include ropy, clast-laden glasses, quench crystallized and vitrophyric glasses, homogeneous glass fragments and spheres, and agglutinates. All of these breccias contain appreciable amounts of glass or quench crystallized glass. Most of this glass is in the categories of ropy, clast-laden, quench crystallized, and vitrophyric. It has been argued that ropy glasses are formed by relatively large impacts and are not related to surface reworking by micrometeorites [*Fruland et al.*, 1977]. Our data would support this interpretation because agglutinate abundances are extremely low for all regolith breccia samples except 63507, yet ropy, clast-laden and quench crystallized glass contents are relatively high, averaging 10.4% (Table 4). The abundances of these glasses is clearly not related to the abundance of agglutinates and therefore it is unlikely that the ropy glasses and related types were formed by micrometeorite reworking; larger impacts are required.

The extremely low maturity of these regolith breccias as reflected by the low agglutinate content is also supported by the low FMR maturity index (I_s/FeO) and low solar wind gas content as discussed in a subsequent section. The correlation of low agglutinate content with low maturity indices based on other techniques shows that the relative lack of agglutinates is a real feature of these regolith breccias and is not an artifact of the breccia-forming process. However, the lack of petrographically identifiable agglutinates in some of the compact Apollo 15 regolith breccias that have appreciable surface maturity based on the FMR index and rare gas content indicates that agglutinates can be severely modified in the breccia-forming event (paper in preparation). This apparently does not occur for porous regolith breccias. It is now generally accepted that regolith breccias in general have significantly lower maturity than typical surface soils or even cores [*Simon et al.*, 1984].

DISAGGREGATION AND GRAIN-SIZE ANALYSIS

As part of our approach to studying regolith breccias, we have developed techniques to disaggregate breccias into their component grains. We are then able to treat the disaggregated breccias as soils and perform a number of analyses on the soil-like material including grain size, rare gas, FMR, and petrographic anlyses of grain-size separates, and SEM analysis of individual grains. Such "pull-apart" studies have the potential of revealing new information about the history and evolution of the regolith represented by the breccias. Data on "pull-apart" breccias can also be directly compared with the large body of data on lunar soils.

We have tried two very different disaggregation techniques. In the freeze-thaw technique a breccia chip sealed in a container with water is alternately frozen and thawed. We used an adaptation of the device described by *Bernatowicz et al.* [1979], who alternatively bathed the sample container in liquid nitrogen and heated water. In our own technique, the breccia chip was heat sealed in a double teflon pouch with distilled water and then automatically cycled between a bath of refrigerated organic liquid (3M Fluorinert FC-77) at –40°C and a bath of warm water at 50°C. Time for one complete freeze-thaw cycle was 3.8 minutes. Total times ranged from 86 hours for 60016 to 315 hours for 61175. Samples were dried and sieved after disaggregation. When completed, the size fractions appeared to contain relatively clean grains closely resembling soil grains of the same size fractions. The second technique consisted of immersing the chips in either Freon or distilled water agitated by a 500W ultrasonic transducer. Disaggregation time was 6.5 hr (Freon) for 60016.

We sieved the diaggregated material at 1000, 500, 250, 150, 90, 45, and 20 μm. Sieve data are presented in Table 5 along with summary grain-size statistics. Histograms of some of the

TABLE 4. Optical Modes for 20–500-μm Particle Types in Apollo 16 Regolith Breccias

Sample	60010	60016	61135	61175	61295	61516	63507
Section Number	6037	171 & 172	8	108	37	4	14
Optical Mode: 20–500 μm (Normalized)							
Monomineralic Fragments							
Plagioclase	45.9	44.5	53.0	40.7	39.0	54.2	17.0
Olivine	2.0	7.3	8.3	2.0	4.0	6.7	2.7
Pyroxene	0.7	1.1	2.0	2.7	2.7	0.0	1.7
Ilmenite	0.0	0.0	0.0	0.3	0.0	0.0	0.0
Spinel	0.0	0.0	0.0	0.0	0.0	0.0	0.0
Troilite	0.0	0.0	0.0	0.0	0.0	0.0	0.0
Metal	0.0	0.0	0.0	0.0	0.0	0.0	0.3
SiO_2	0.0	0.0	0.0	0.0	0.3	0.0	0.0
(Subtotal)	(48.5)	(52.9)	(63.3)	(45.7)	(46.0)	(60.8)	(21.7)
Crystalline Lithics							
Anorthosite	1.3	7.8	6.3	8.7	12.3	5.8	6.7
Norite-Troctolite	1.3	2.1	2.7	1.7	0.7	3.3	2.7
Mare Basalt	0.0	0.0	0.0	0.0	0.0	0.0	0.0
KREEP Basalt	0.0	0.0	0.7	1.3	0.0	0.0	0.0
Other/Indet	4.6	4.7	5.3	6.7	7.0	6.7	2.7
(Subtotal)	(7.2)	(14.6)	(15.0)	(18.3)	(20.0)	(15.8)	(12.0)
Breccias							
Regolith Porous	0.0	0.0	0.0	0.0	0.0	0.0	0.0
Regolith Compact	0.0	0.0	0.0	0.0	0.0	0.0	0.0
Vitric Porous	0.0	0.0	0.0	0.0	0.0	0.0	0.0
Vitric Compact	0.3	5.2	0.7	1.7	1.0	1.7	2.0
Fragmental Porous	0.0	0.5	0.7	0.0	0.0	0.0	0.7
Fragmental Compact	0.0	0.0	0.0	0.0	0.0	0.0	0.0
(Subtotal)	(0.3)	(5.8)	(1.3)	(1.7)	(1.0)	(1.7)	(2.7)
Crystalline/Melt Matrix							
Poik., Eq. Plag.	1.3	3.7	2.3	0.3	2.7	3.3	1.3
Poik., Acic. Plag.	0.0	0.0	0.0	0.7	0.0	0.0	0.0
Variolitic	0.0	0.0	0.0	0.7	1.0	0.0	0.0
Subophitic	8.2	3.7	5.0	7.3	9.7	6.7	9.7
Intergranular	1.0	4.2	2.7	4.0	3.0	1.7	10.7
Intersertal	0.0	0.0	0.3	0.0	0.3	2.5	0.0
Porphyritic	0.0	0.0	0.0	0.0	0.0	0.0	0.0
Granulitic	0.3	0.0	0.0	3.0	0.0	0.0	0.7
(Subtotal)	(10.8)	(11.5)	(10.3)	(16.0)	(16.7)	(14.2)	(22.3)
Glasses							
Inhomogeneous							
Clastic/Ropy	2.3	3.7	6.3	7.3	5.7	3.3	8.3
Quenched/Vitrophyric	3.3	6.3	3.3	4.7	3.7	0.0	6.7
(Subtotal)	(5.6)	(10.0)	(9.7)	(12.0)	(9.3)	(3.3)	(15.0)
Homogeneous							
Green	0.0	0.0	0.0	0.0	0.0	0.0	0.0
Yellow	0.0	0.0	0.0	0.3	0.0	0.0	0.3
Colorless/Gray	0.7	2.6	0.3	2.3	4.0	0.8	1.7
Black/Orange	1.0	1.6	0.0	0.7	1.0	0.0	0.0
(Subtotal)	(1.6)	(4.2)	(0.3)	(3.3)	(5.0)	(0.8)	(2.0)
Regolith Components							
Spheres	0.0	0.5	0.0	0.0	0.7	0.0	0.7
Agglutinates	25.9	0.5	0.0	3.0	1.3	3.3	23.7
(Subtotal)	(25.9)	(1.0)	(0.0)	(3.0)	(2.0)	(3.3)	(24.3)
Total	100.0	100.0	100.0	100.0	100.0	100.0	100.0

Table 4. (continued)

Sample	63588	63595	65095	65715	66035	66036	66075
Section Number	5	8	54	5	14	13	70
Optical Mode: 20–500 μm (Normalized)							
Monomineralic Fragments							
Plagioclase	43.3	54.3	44.9	47.7	41.4	43.7	57.7
Olivine	5.0	5.7	2.7	6.5	8.5	8.0	6.0
Pyroxene	4.3	0.0	1.7	1.0	0.0	0.0	4.0
Ilmenite	0.0	0.0	0.0	0.0	0.0	0.0	0.0
Spinel	0.0	0.0	0.0	0.0	0.0	0.0	0.0
Troilite	0.3	0.0	0.0	0.0	0.0	0.0	0.0
Metal	0.3	0.0	0.3	0.0	0.0	0.0	0.0
SiO_2	0.0	0.0	0.0	0.0	0.0	0.0	0.3
(Subtotal)	(53.3)	(59.9)	(49.5)	(55.2)	(49.9)	(51.7)	(68.0)
Crystalline Lithics							
Anorthosite	7.3	6.9	3.09	6.5	6.0	5.3	0.7
Norite-Troctolite	5.3	3.2	0.7	2.3	2.1	2.3	1.3
Mare Basalt	0.0	0.0	0.0	0.0	0.0	0.0	0.0
KREEP Basalt	0.0	0.0	0.0	0.0	3.2	0.0	0.3
Other/Indet	4.3	6.9	9.6	7.5	7.5	10.7	3.0
(Subtotal)	(17.0)	(17.0)	(13.3)	(16.4)	(18.8)	(18.3)	(5.3)
Breccias							
Regolith Porous	0.0	0.0	0.0	0.0	0.0	0.0	0.0
Regolith Compact	0.0	0.0	4.3	0.0	0.0	0.0	0.0
Vitric Porous	0.0	0.0	0.0	0.0	0.0	0.0	0.0
Vitric Compact	4.3	3.2	0.0	0.0	0.0	2.0	5.0
Fragmental Porous	0.0	0.3	0.0	0.0	0.0	0.0	0.0
Fragmental Compact	0.3	0.0	0.3	0.0	0.0	0.0	0.0
(Subtotal)	(4.7)	(3.5)	(4.7)	(0.0)	(0.0)	(2.0)	(5.0)
Crystalline/Melt Matrix							
Poik., Eq. Plag.	2.7	2.2	10.0	3.3	8.8	6.3	4.0
Poik., Acic. Plag.	0.0	0.6	0.0	0.0	0.0	0.0	0.0
Variolitic	0.0	0.0	0.0	0.0	0.0	0.0	0.0
Subophitic	3.7	1.9	8.6	4.6	7.5	3.9	4.3
Intergranular	2.0	3.8	2.7	2.9	0.0	4.0	1.7
Intersertal	0.0	0.0	0.0	0.0	0.0	0.0	0.7
Porphyritic	0.0	0.0	0.0	0.0	0.0	0.0	0.0
Granulitic	0.7	0.0	1.0	0.7	0.0	0.3	0.3
(Subtotal)	(9.0)	(8.5)	(22.3)	(11.4)	(16.4)	(13.7)	(11.0)
Glasses							
Inhomogeneous							
Clastic/Ropy	3.3	5.1	6.0	9.8	5.3	5.3	2.3
Quenched/Vitrophyric	11.0	3.8	4.3	3.9	2.2	6.7	7.3
(Subtotal)	(14.3)	(8.8)	(10.3)	(13.7)	(7.5)	(12.0)	(9.7)
Homogeneous							
Green	0.0	0.0	0.0	0.0	0.0	0.0	0.0
Yellow	0.0	0.0	0.0	0.3	0.0	0.0	0.0
Colorless/Gray	1.3	1.6	0.0	2.6	3.2	0.3	0.0
Black/Orange	0.0	0.3	0.0	0.0	0.0	0.7	0.0
(Subtotal)	(1.3)	(1.9)	(0.0)	(2.9)	(3.2)	(1.0)	(0.0)
Regolith Components							
Spheres	0.3	0.3	0.0	0.3	3.2	0.3	1.0
Agglutinates	0.0	0.0	0.0	0.0	1.1	1.0	0.0
(Subtotal)	(0.3)	(0.3)	(0.0)	(0.3)	(4.2)	(1.3)	(1.0)
Total	100.0	100.0	100.0	100.0	100.0	100.0	100.0

Approximately 300 points falling on particles in the 20–500-μm size range were identified and counted for most thin sections. Points that fell on matrix, particles smaller than 20 μm, or particles larger than 500 μm were not counted in the 300 points; except for several sections that were not large enough, actual number of points identified on each thin section was approximately 800. Petrographic descriptions of the classification scheme used is given in Appendix 1.

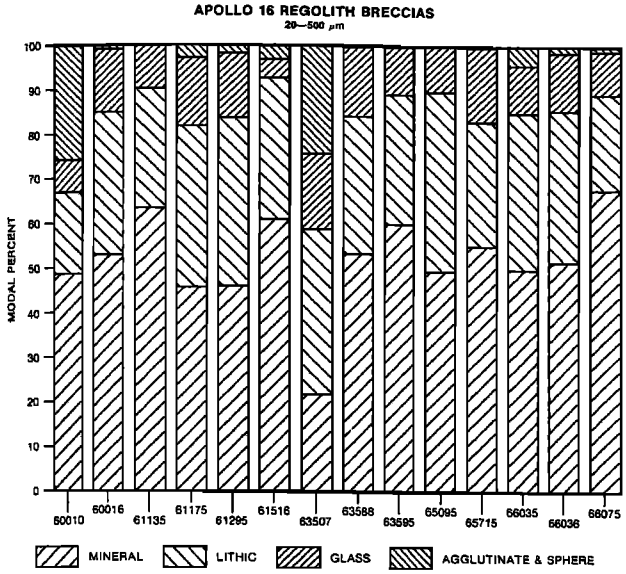

Fig. 1. Modal percent of major components in point-counted Apollo 16 regolith breccia thin sections and in one continuous thin section from core sample 60010. Min category includes plagioclase, pyroxene, olivine, and other minerals; lithic category includes all crystalline lithics and breccias; Glass category includes quenched, clast-bearing, inhomogeneous, and homogeneous varieties of fragmental glass; agglutinates and spheres include all glassy and quenched-crystallized sphere and fragments of spheres.

grain-size distributions are shown in Figure 3. For comparison, breccia 14301 data from *Bernatowicz et al.* and several soils are also shown. Several points should be noted. First, the disaggregation techniques appear to have disaggregated the breccias into size distributions that are mostly similar to typical soils. *Quaide and Bunch* [1970] first pointed out the similarity between the grain-size distribution of Apollo 11 regolith breccias and soil. All of our disaggregated Apollo 16 breccias have nearly log normal distributions as do most soils. For example, breccia 61175 (freeze-thaw) is very similar in its grain-size parameters to submature soil 63321 except that the breccia is slightly deficient in coarser fragments compared to the soil suggesting a somewhat more mature size distribution. This breccia cannot be distinguished from a typical soil based on the grain-size parameters. The ultrasonic version of 60016 closely resembles the freeze-thaw version showing that for this breccia the size distribution is relatively independent of the disaggregation technique.

The grain-size distributions of the Apollo 16 breccias more closely resemble those of mature soils than they do immature soils; the disaggregated breccias have relatively low standard deviations and lack bimodal distributions, although the sample size used (typically 0.5 g) would preclude the inclusion of many larger fragments. Additionally, the samples were chosen to be mainly matrix and to avoid obvious clasts. Consequently, a coarse bimodal component may be present but would be missed by the sampling.

Polished grain mounts of size fractions of the disaggregated breccias were prepared and about 300 grains were identified and tabulated from each size fraction (Table 6). A weighted average of the size fractions was made to determine the overall particle population in the 20–500-μm-size range. Table 7 and Figure 4 show some of the petrographic data for the disaggregated grain mounts of 60016 compared to the modal analysis of the 20–500-μm-size range for the polished thin section of the original aggregated breccia. The correspondence between the two techniques is good. Mineral grain abundances are similar, with plagioclase numbers nearly identical. Lithic fragment abundances are also similar. The low values for fragmental porous breccia fragments in the disaggregated samples indicate that disaggregation was efficient because 60016 is itself a porous fragmental breccia. An important conclusion from Table 6 is that the disaggregation did not significantly modify the petrologic composition of the breccia, supporting the suggestion that the analyzed grain-size distribution represents the grain-size distribution of the original fragmental material from which the breccias were made. Overall, the modal composition of 60016 is similar to typical Apollo 16 soils with the notable exception that it contains only trace amounts of agglutinates and glass spheres compared to soils.

Noble Gases, I_s/FeO, and Surface Maturity

Small chips of 19 Apollo 16 regolith breccias, each weighing 20 to 75 mg, were analyzed for noble gas isotopes by mass spectrometry using standard techniques. In addition we analyzed the <20-μm and 90–150-μm size fractions of disaggregated breccias 60016 and 61175, the former breccia being disaggregated by both the freeze-thaw and ultrasonic techniques. The measured noble gas isotopic abundances are given in Table 8.

Chips weighing between 5 and 30 mg each were analyzed by FMR and static magnetic techniques to determine values of I_s and concentrations of metallic iron (FeO), respectively. I_s is the specific intensity of the resonance at g + 2.1 that is due to fine-grained metal formed by exposure-induced reduction of FeO. The magnitude of I_s/FeO has been shown for lunar soils to be proportional to the duration of surface exposure

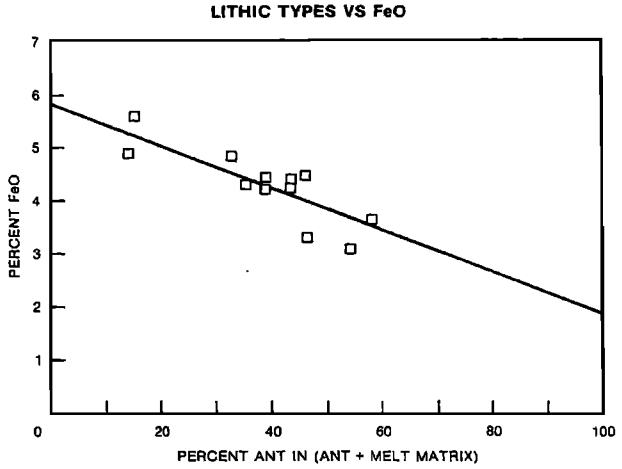

Fig. 2. Variation of FeO (wt %) with major lithic types from Table 4. For this figure, all lithic types in the anorthosite, norite, troctolite, and crystalline melt matrix categories were combined and the percentage of that combined category belonging to anorthosites, norites, and troctolites (ANT) was determined. That percentage is plotted against FeO. Regolith breccia 63507 was omitted from the plot because it has an anomolously high contribution of meteoritic material to the FeO (see text). The line shown is a least squares fit with a correlation R = 0.80. Extrapolation of this line to 0% ANT gives an FeO content of 5.90% for the melt matrix breccia suite. Extrapolation to 100% gives an FeO content of 1.88 for the ANT suite.

TABLE 5. Grain Size Parameters for Disaggregated Regolith Breccias

Sample	60016,165		60016,165	
Technique	Freeze-Thaw		Ultrasonic	
Mean Grain Size (M_z)	67 μm		74 μm	
Standard Deviation (S_g)	2.32 phi		3.05 phi	
Grain Size	Weight (gm)	Weight %	Weight (gm)	Weight %
>1000 μm	0.01691	4.78	0.06879	13.24
500–1000 μm	0.03131	8.86	0.03442	6.63
250–500 μm	0.03364	9.51	0.04662	8.98
150–250 μm	0.03116	8.81	0.04063	7.82
90–150 μm	0.03546	10.03	0.04221	8.13
45–90 μm	0.05947	16.82	0.06529	12.57
20–45 μm	0.05912	16.72	0.07955	15.32
<20 μm	0.08652	24.47	0.14184	27.31
Total	0.35359	100.00	0.51935	100.00
Sample	61175,207		66075,16	
Technique	Freeze Thaw		Freeze Thaw	
Mean Grain Size (M_z)	44 μm		56 μm	
Standard Deviation (S_g)	2.73 phi		1.80 phi	
Grain Size	Weight (gm)	Weight %	Weight (gm)	Weight %
>1 mm	0.00438	1.04	0.00320	0.60
500–1000 μm	0.02860	6.77	0.02379	4.48
250–500 μm	0.04235	10.02	0.04104	7.72
150–250 μm	0.03772	8.93	0.04393	8.27
90–150 μm	0.05097	12.07	0.06031	11.35
45–90 μm	0.04930	11.67	0.12662	23.83
20–45 μm	0.07072	16.74	0.12096	22.76
<20 μm	0.13839	32.76	0.11151	20.99
Total	0.42243	100.0	0.53136	100.00

Breccias were disaggregated using freeze-thaw or ultrasonic techniques (see text). Breccias were sieved, and summary statistical parameters were determined using techniques developed for lunar soils [*McKay, et al.* 1974].

[*Morris*, 1976, 1978]. Values of I_s/FeO (calculated using our chemically determined FeO concentrations) and FeO concentrations are given in Table 9.

All 19 breccias, except 65095, contain gases of obvious solar wind origin, but generally in much lower concentrations than found in Apollo 16 soils or in typical regolith breccias from mare sites. Most of these breccias show very low I_s/FeO values of less than 1, which is lower than virtually all soils in the Apollo collection [*Morris*, 1978]. At such low levels of I_s/FeO it is possible that not all of the value of I_s is due to processes correlated with surface exposure. Figure 5 compares the two surface maturity parameters, I_s/FeO and solar ^{36}Ar concentrations, for these Apollo 16 breccias and for 28 Apollo 15 regolith breccias [*Bogard et al.*, 1985]. The range of solar ^{36}Ar concentrations is shown for typical Apollo 15 and 16 soils. The I_s/FeO values for lunar soils would typically fall in the range of 20 to 90 [*Morris*, 1978]. Breccia 63507 has I_s/FeO and ^{36}Ar values of typical submature soils and also contains by far the largest agglutinate concentration of any of these breccias. Breccia 63507 contains unusually large concentrations of siderophile elements, suggesting an appreciable meteoritic component (discussed in the next section). Breccias 60255, 61536, 61175, and 61295 have ^{36}Ar concentrations and I_s/FeO values similar to the most immature Apollo 16 soils known (e.g., 61221 and $I_s/FeO = 9$). These breccias contain very small, but measurable, agglutinate concentrations. Fourteen of the Apollo 16 breccias have I_s/FeO values and ^{36}Ar concentrations far less than any known Apollo 16 soil. The agglutinate concentrations of these breccias are very low, generally less than 1%. Thirteen of these 14 breccias, however, contain obvious components produced by surface irradiation, i.e., solar noble gases and fine-grained metal, but the amounts of these components are considerably smaller than any other known group of lunar regolith breccias.

The noble gas concentrations and I_s/FeO values in grain-size separates for breccias 60016 and 61175 have several times larger concentrations in the <20-μm fraction than the 90–150-μm fraction, indicating that the solar component is concentrated in grain surfaces. The same effect is observed for lunar soils and demonstrates that the solar gases and the fine-grained metal in these breccias were acquired while a portion of the breccia lay finely disseminated on the lunar surface and was irradiated by the solar wind. The concentrations of solar gases as a function of grain size is approximately the same as is observed in soils and suggests that the techniques used to disaggregate these breccias essentially reproduced the original grain-size distribution that existed during irradiation.

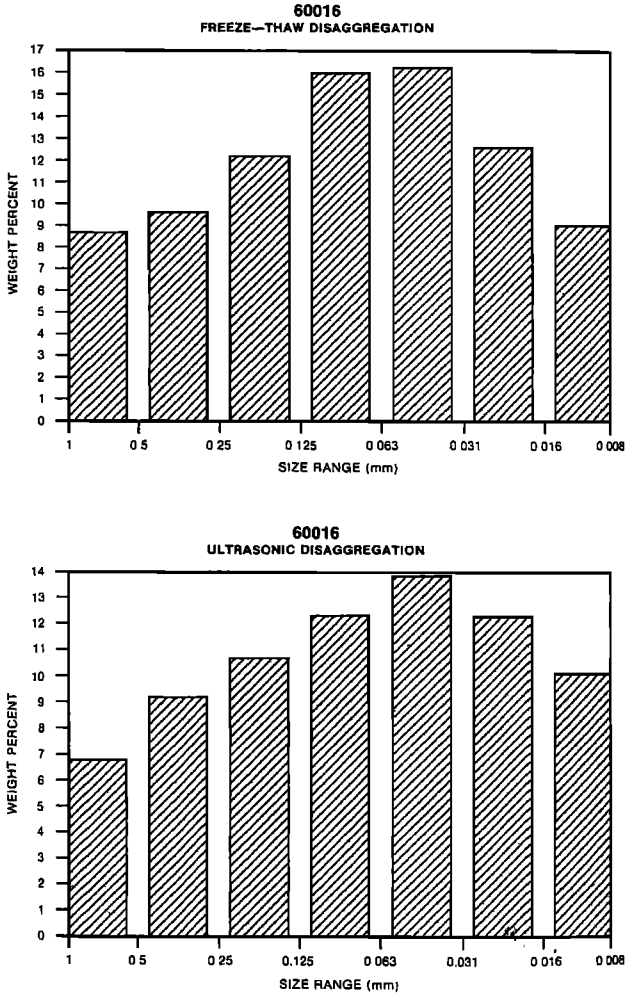

Fig. 3*a*

Fig. 3. Grain-size histograms for disaggregated Apollo 16 regolith breccias, an Apollo 14 disaggregated regolith breccia, and a submature Apollo 16 soil. Size intervals range from zero phi (1 mm) to 7 phi (8 μm). (*a*) Compares 60016 freeze-thaw with 60016 ultrasonically disaggregated, (*b*) presents freeze-thaw data on 61176 and 66075, (*c*) shows size distribution on 14301 from data of *Bernatowicz et al.* [1979] and data on soil 63321.

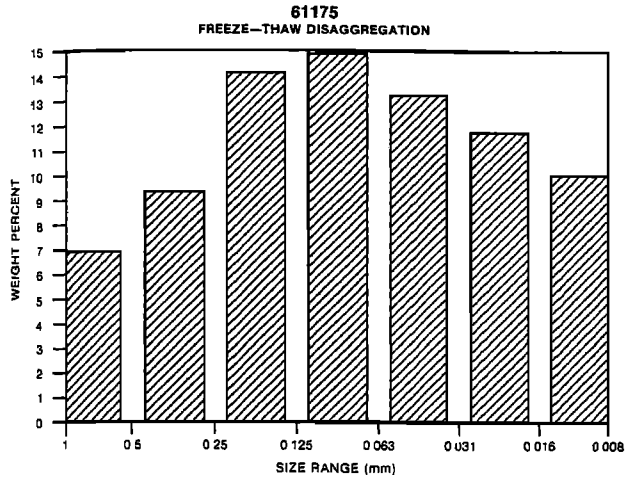

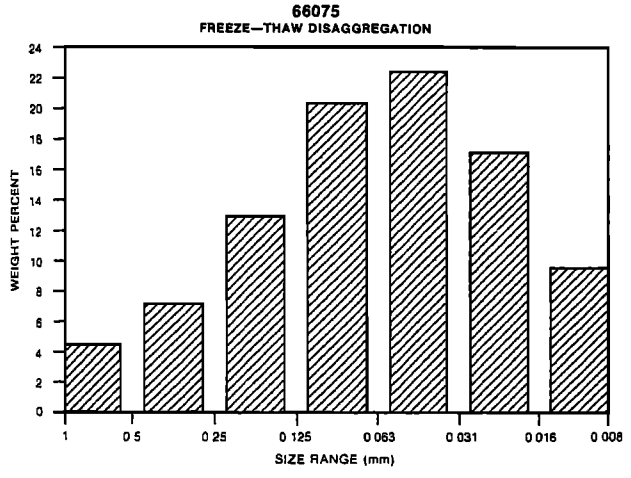

Fig. 3*b*

It is informative to compare the surface maturity indices, I_s/FeO and ^{36}Ar concentrations, of these Apollo 16 breccias with those for meteorite breccias. The data for the Allan Hills 81005 lunar meteorite is shown in Figure 5. The surface maturity shown by Allan Hills 81005 [*Morris*, 1983; *Bogard and Johnson*, 1983] is in the low range for a lunar soil but plots in the upper range for these Apollo 16 breccias. This lunar meteorite has been compared petrochemically to two of these breccias, 60016 and 60019 [*Takeda et al.*, 1985], but it shows considerably higher surface maturity than these two Apollo 16 breccias. Among nonlunar meteorites that show evidence of surface irradiation in a regolith, the Fayetteville chondrite has the largest measured concentrations of solar wind ^{36}Ar [*Schultz and Kruse*, 1978] and thus presumably experienced the greatest amount of surface irradiation. Various analyses of Fayetteville gave a range of ^{36}Ar concentrations of about $1\text{–}6 \times 10^{-6}$ cm^3/g, and a preliminary I_s/FeO value for Fayetteville is approximately zero. Thus the degrees of solar wind irradiation and micrometeorite bombardment shown by the "gas-rich" brecciated meteorites are less than those for these Apollo 16 breccias.

Most of those Apollo 16 breccias with low concentrations of ^{36}Ar also appear to have experienced little, if any, irradiation by cosmic rays. The $^{21}Ne/^{22}Ne$ ratio for solar gas trapped in lunar soils typically varies in the range of 0.031 to 0.033 because of mass fractionation during partial gas loss. This ratio can increase substantially when irradiation by cosmic rays produces cosmogenic Ne within silicate materials. The Ne isotopic composition of most of the Apollo 16 breccias would be sensitive to cosmic ray irradiation. Yet 10 of those breccias with low concentrations of solar gases also show $^{21}Ne/^{22}Ne$ ratios of 0.031 to 0.033, suggesting that any cosmic ray irradiation has been limited to no more than a few million years. (Lunar soils commonly show total cosmic ray irradiation times of hundreds of millions of years.) The cosmic ray exposure age of 60016 has been estimated as ~2 m.y. and this breccia may have been exposed by the South Ray crater event, which apparently initiated cosmic ray exposure of several other rocks [*Weber and Schultz*, 1978]. A few breccias do have $^{21}Ne/^{22}Ne$ ratios considerably greater than 0.033 and have experienced significant irradiation by cosmic rays. There is some tendency for increasing $^{21}Ne/^{22}Ne$ due to cosmic ray irradiation to increase proportionally to solar ^{36}Ar concentrations, suggesting that a common phase in these breccias may carry both gas components.

Excess ^{40}Ar and Fission Xe

The isotopic composition of the solar gases in these breccias closely resembles solar gases found in typical lunar soils, except that several breccias show unusually large $^{40}Ar/^{36}Ar$ ratios and excessive abundances of heavy isotopes of Xe relative to the

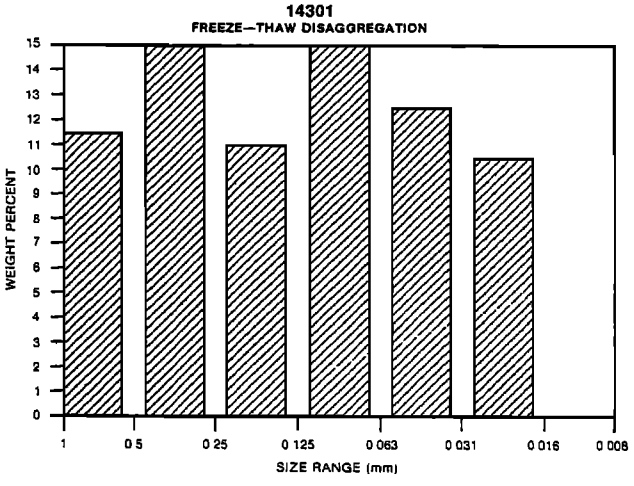

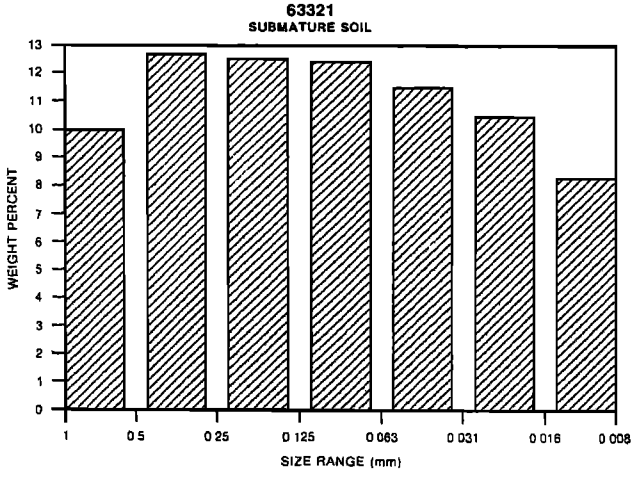

Fig. 3*c*

TABLE 6. Grain Populations from Polished Grain Mounts of Disaggregated Size Fractions of Regolith Breccia 60016

Sample	60016	60016	60016	60016	60016	60016
Section No.	165 FT	165 FT	165 FT	165 FT	165 FT	165 FT
Size Fraction (μm)	500–1000	250–500	150–250	90–150	45–90	20–45
No. of Grains	14	144	261	300	300	300
	Optical Modes: Disaggregated 60016 Grain Mounts					
Monomineralic Fragments						
Plagioclase	7.1	16.0	26.8	40.0	51.7	61.7
Olivine	0.0	0.0	0.0	2.3	8.3	12.0
Pyroxene	0.0	1.4	1.9	3.3	2.0	5.3
Ilmenite	0.0	0.0	0.0	0.0	0.0	0.3
Spinel	0.0	0.0	0.0	0.0	0.0	0.0
Troilite	0.0	0.0	0.0	0.0	0.0	0.3
Metal	0.0	0.0	0.0	0.3	0.0	0.0
SiO_2	0.0	0.0	0.0	0.0	0.0	0.0
(Subtotal)	(7.1)	(17.4)	(28.7)	(46.0)	(62.0)	(79.7)
Crystalline Lithics						
Anorthosite	7.1	16.7	13.0	8.0	3.0	0.0
Norite-Troctolite	7.1	6.9	5.0	2.7	0.3	0.0
Mare Basalt	0.0	0.0	0.0	0.0	0.0	0.0
KREEP Basalt	0.0	0.0	0.0	0.0	0.0	0.0
Other/Indet.	0.0	0.0	0.0	0.3	0.0	2.3
(Subtotal)	(14.3)	(23.6)	(18.0)	(11.0)	(3.3)	(2.3)
Breccias						
Regolith Porous	0.0	0.0	0.0	0.0	0.0	0.0
Regolith Compact	0.0	0.0	0.0	0.0	0.0	0.0
Vitric Porous	0.0	0.0	0.0	0.0	0.0	0.0
Vitric Compact	14.3	6.2	3.8	1.0	1.3	0.3
Fragmental Porous	0.0	0.0	1.5	1.3	4.7	0.7
Fragmental Compact	14.3	2.8	2.3	0.0	0.3	0.3
(Subtotal)	(28.6)	(9.0)	(7.7)	(2.3)	(6.3)	(1.3)
Crystalline/Melt Matrix						
Poik., Eq. Plag.	7.1	6.3	4.6	3.7	0.7	0.0
Poik., Acic. Plag.	7.1	2.1	0.8	0.3	0.0	0.0
Variolitic	0.0	1.4	0.0	0.0	0.0	0.0
Subophitic	28.6	16.7	16.1	7.7	8.3	4.3
Intergranular	0.0	4.2	4.2	2.3	2.7	0.0
Intersertal	0.0	0.7	0.4	0.0	0.0	0.0
Porphyritic	0.0	0.0	0.0	0.0	0.0	0.0
Granulitic	7.1	1.4	0.4	0.7	0.0	0.0
(Subtotal)	(50.0)	(32.6)	(26.4)	(14.7)	(11.7)	(4.3)
Glasses						
Inhomogeneous						
Clastic/Ropy	0.0	4.9	3.1	8.7	2.7	4.3
Quenched/Vitrophyric	0.0	11.8	15.3	15.3	11.7	6.3
(Subtotal)	(0.0)	(16.7)	(18.4)	(24.0)	(14.3)	(10.7)
Homogeneous						
Green	0.0	0.0	0.0	0.0	0.0	0.0
Yellow	0.0	0.0	0.0	0.0	0.0	0.0
Colorless/Gray	0.0	0.0	0.0	1.7	1.3	1.3
Black/Orange	0.0	0.0	0.0	0.0	0.0	0.0
(Subtotal)	(0.0)	(0.0)	(0.0)	(1.7)	(1.3)	(1.3)
Regolith Components						
Spheres	0.0	0.7	0.0	0.3	1.0	0.0
Agglutinates	0.0	0.0	0.8	0.0	0.0	0.3
(Subtotal)	(0.0)	(0.7)	(0.8)	(0.3)	(1.0)	(0.3)
Total	100.0	100.0	100.0	100.0	100.0	100.0

TABLE 6. (continued)

Sample	60016	60016	60016	60016	60016	60016
Section No.	165 S	165 S	165 S	165 S	165 S	165 S
Size Fraction (μm)	500–1000	250–500	150–250	90–150	45–90	20–45
No. of Grains	9	113	154	300	300	300
Monomineralic Fragments						
Plagioclase	0.0	15.9	29.9	42.0	55.7	59.0
Olivine	0.0	0.0	2.0	6.0	8.0	14.7
Pyroxene	0.0	1.8	2.6	2.0	3.0	4.3
Ilmenite	0.0	0.0	0.0	0.0	0.0	0.7
Spinel	0.0	0.0	0.0	0.0	0.0	0.3
Troilite	0.0	0.0	0.0	0.0	0.0	0.0
Metal	0.0	0.0	0.7	0.0	0.0	0.0
SiO_2	0.0	0.0	0.0	0.0	0.0	0.0
(Subtotal)	(0.0)	(17.7)	(35.1)	(50.0)	(66.7)	(79.0)
Crystalline Lithics						
Anorthosite	33.3	6.2	4.6	7.0	3.7	0.0
Norite-Troctolite	11.1	3.5	2.0	3.0	0.7	0.0
Mare Basalt	0.0	0.0	0.0	0.0	0.0	0.0
KREEP Basalt	0.0	0.0	0.0	0.0	0.0	0.0
Other/Indet.	0.0	0.0	0.0	0.0	0.0	6.3
(Subtotal)	(44.4)	(9.7)	(6.5)	(10.0)	(4.3)	(6.3)
Breccias						
Regolith Porous	0.0	0.0	0.0	0.0	0.0	0.0
Regolith Compact	0.0	0.0	0.0	0.0	0.0	0.0
Vitric Porous	0.0	0.0	0.0	0.0	0.0	0.0
Vitric Compact	0.0	0.0	0.0	0.0	0.0	0.0
Fragmental Porous	0.0	7.1	5.2	1.0	0.7	0.7
Fragmental Compact	0.0	0.9	0.0	1.3	0.7	0.0
(Subtotal)	(11.1)	(21.2)	(9.7)	(4.3)	(4.0)	(0.7)
Crystalline/Melt Matrix						
Poik., Eq. Plag.	11.1	9.7	3.9	1.3	0.7	0.7
Poik., Acic. Plag.	0.0	2.7	0.0	0.0	0.0	0.0
Variolitic	0.0	0.0	0.0	0.0	0.0	0.0
Subophitic	11.1	14.2	15.6	11.7	5.7	0.3
Intergranular	0.0	1.8	5.2	1.7	1.3	0.0
Intersertal	11.1	0.9	0.0	0.0	0.0	0.0
Porphyritic	0.0	0.0	0.0	0.0	0.0	0.0
Granulitic	0.0	1.8	0.7	0.7	1.0	0.7
(Subtotal)	(33.3)	(31.0)	(25.3)	(15.3)	(8.7)	(1.7)
Glasses						
Inhomogeneous						
Clastic/Ropy	0.0	2.7	3.9	7.0	4.7	2.3
Quenched/Vitrophyric	11.1	16.8	17.5	9.3	9.3	6.0
(Subtotal)	(11.1)	(19.5)	(21.4)	(16.3)	(14.0)	(8.3)
Homogeneous						
Green	0.0	0.0	0.0	0.0	0.0	0.0
Yellow	0.0	0.0	0.0	0.0	0.0	0.0
Colorless/Gray	0.0	0.9	0.7	1.3	0.7	2.7
Black/Orange	0.0	0.0	0.0	0.3	0.0	0.0
(Subtotal)	(0.0)	(0.9)	(0.7)	(1.7)	(0.7)	(2.7)
Regolith Components						
Spheres	0.0	0.0	1.3	2.3	1.0	1.3
Agglutinates	0.0	0.0	0.0	0.0	0.7	0.0
(Subtotal)	(0.0)	(0.0)	(1.3)	(2.3)	(1.7)	(1.3)
Total	100.0	100.0	100.0	100.0	100.0	100.0

Grain mounts of both the freeze-thaw disaggregated and the ultrasonically disaggregated size fractions are included for comparison. Petrographic descriptions of the classification scheme used are given in Appendix 1.

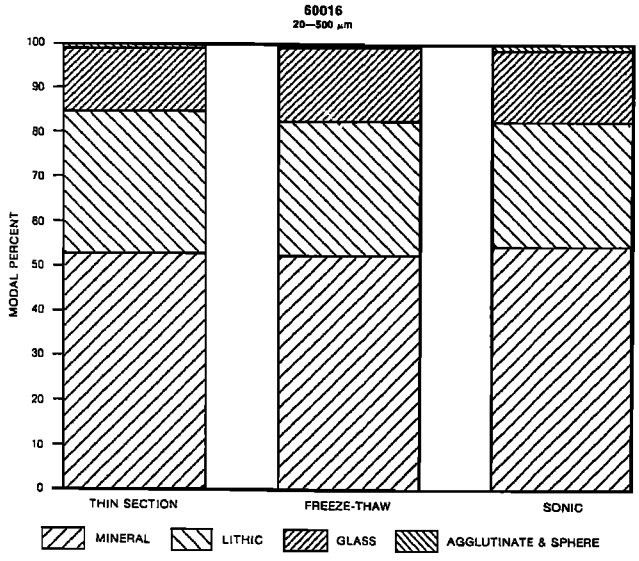

Fig. 4. A comparison of modal data on the 20–500-μm size interval from thin sections of regolith breccia 60016 to grain population data from grain mounts of size fractions for disaggregated versions of 60016 produced by both the freeze-thaw (FT) technique and the ultrasonic (SONIC) technique. Data on the disaggregated samples are weighted averages from five size intervals ranging from 20 to 500 μm. Particle categories are the same ones used in Figure 1.

lighter Xe isotopes. These enhanced abundances of ^{40}Ar and heavy Xe can give evidence as to the time of solar irradiation and possible breccia formation. We have calculated the trapped $^{40}Ar/^{36}Ar$ ratios for the Apollo 16 regolith breccias (Table 9). These trapped ratios were corrected for ^{40}Ar due to in situ decay of ^{40}K by using the reported K concentrations [*Ryder and Norman*, 1980] and an assumed age of 4 b.y. For those few breccias where K data are not available, we assumed a K concentration of 0.10%, which is the average value of several of these breccias and of several Apollo 16 soils. This calculation does not yield a precise value for trapped $^{40}Ar/^{36}Ar$, but we expect that they are accurate to 30%. Ordinate-intercept plots [*Eberhardt et al.*, 1972] of the Ar data for grain size separates of breccias 60016 and 61175 give more accurate trapped $^{40}Ar/^{36}Ar$ values of 9.2 and 4.1, respectively. Seventeen of the breccias with trapped Ar show corrected $^{40}Ar/^{36}Ar$ in two groups, from 2.5 to about 4 and from 9 to 12.5. The five breccias with the largest ^{36}Ar concentrations all have $^{40}Ar/^{36}Ar$ of about 4 or less, whereas, those nine breccias with isotopic ratios of ~9–12 all have $I_s/FeO < 1$ and show little, if any, cosmic ray irradiation.

Most ^{40}Ar in the lunar regolith is not a component of the solar wind, but is believed to be radiogenic Ar that has escaped from the lunar crust into the lunar atmosphere and has been ionized, accelerated, and implanted into the lunar surface so as to mimic gas implanted by the solar wind [*Manka and Michel*, 1970]. A generally accepted model is that the $^{40}Ar/^{36}Ar$ ratio implanted into the lunar regolith was considerably higher in the distant past when greater amounts of ^{40}K were decaying to ^{40}Ar in the crust [*Yaniv and Heymann*, 1972]. Argon in most lunar soils has a $^{40}Ar/^{36}Ar$ ratio of 0.5 to 1.5 and for some immature, recently exposed soils could only represent recent solar wind irradiation. Many Apollo 16 soils give ratios of about 1 or higher, whereas soils from mare sites commonly give values of about 0.5–1. An apparent higher $^{40}Ar/^{36}Ar$ for some Apollo 16 soils compared to soils from other sites could be due to differences in retention of ^{40}Ar and ^{36}Ar because of soil chemistry or degree of soil reworking (maturation), or the Apollo 16 soils could contain a "primitive" Ar component. Several more

TABLE 7. A Comparison of Grain Populations for Breccia 60016

Sample	Thin Section 60016	Freeze/Thaw 60016	Ultrasonic 60016
Section Number	171 and 172	165	165
Optical Mode: 20–500 μm (Normalized)			
Monomineralic Fragments			
Plagioclase	44.5	43.5	44.0
Olivine	7.3	5.9	7.4
Pyroxene	1.1	3.0	3.0
Ilmenite	0.0	0.1	0.2
Spinel	0.0	0.0	0.1
Troilite	0.0	0.1	0.0
Metal	0.0	0.1	0.1
SiO_2	0.0	0.0	0.0
(Subtotal)	(52.9)	(52.6)	54.7)
Crystalline Lithics			
Anorthosite	7.8	6.5	3.7
Norite-Troctolite	2.1	2.3	1.5
Mare Basalt	0.0	0.0	0.0
KREEP Basalt	0.0	0.0	0.0
Other/Indet	4.7	0.7	1.8
(Subtotal)	(14.6)	(9.5)	(7.0)
Breccias			
Regolith Porous	0.0	0.0	0.0
Regolith Compact	0.0	0.0	0.0
Vitric Porous	0.0	0.0	0.0
Vitric Compact	5.2	2.1	3.9
Fragmental Porous	0.5	1.9	2.5
Fragmental Compact	0.0	0.9	0.5
(Subtotal)	(5.8)	(4.9)	(6.9)
Crystalline/Melt Matrix			
Poik., Eq. Plag.	3.7	2.4	2.8
Poik., Acic. Plag.	0.0	0.5	0.5
Variolitic	0.0	0.2	0.0
Subophitic	3.7	9.5	8.0
Intergranular	4.2	2.3	1.6
Intersertal	0.0	0.2	0.2
Porphyritic	0.0	0.0	0.0
Granulitic	0.0	0.4	0.9
(Subtotal)	(11.5)	(15.5)	(14.0)
Glasses			
Inhomogeneous			
Clastic/Ropy	3.7	4,5	3.9
Quenched/Vitroph	6.3	11.4	10.9
(Subtotal)	(10.0)	(15.9)	(14.8)
Homogeneous			
Green	0.0	0.0	0.0
Yellow	0.0	0.0	0.0
Colorless/Gray	2.6	1.0	1.4
Black/Orange	1.6	0.0	0.1
(Subtotal)	(4.2)	(1.0)	(1.4)
Regolith Components			
Spheres	0.5	0.4	1.2
Agglutinates	0.5	0.2	0.2
(Subtotal)	(1.0)	(0.6)	(1.3)
Total	100.0	100.0	100.0

Grain populations in the disaggregated grain mounts of 60016 are compared to modal data from thin sections of the nondisaggregated breccia for the size interval from 20 to 500 μm. For the disaggregated samples, the 20–500-μm data in this table is a weighted average of all of the size fraction data in Table 6. Petrographic descriptions of the classification scheme used are given in Appendix 1.

TABLE 8. Isotopic Concentrations (cm^3 STP/g) of Noble Gases in Apollo 16 Regolith Breccias

Breccia	Wt. mg	^{3}He E-7	^{4}He E-4	^{22}Ne E-6	^{20}Ne/^{22}Ne	^{21}Ne/^{22}Ne E-2	^{36}Ar E-6	^{36}Ar/^{38}Ar	^{40}Ar/^{36}Ar	^{84}Kr E-9	^{132}Xe E-9
60016,165	35.2	2.77	11.0	1.56	12.26±.02	3.30±.05	6.89	5.261±.005	20.22±.03	2.01	0.55
<20-FT	19.0	20.3	53.7	7.26	12.36±.02	3.10±.02	26.1	5.252±.005	10.72±.05	13.2	2.58
<20-US	9.7	18.4	47.4	6.89	12.38±.02	3.17±.03	25.5	5.247±.005	10.73±.03	13.4	2.61
90–150 FT	22.6	0.91	3.97	0.46	11.96±.04	4.01±.05	2.29	5.102±.005	25.07± .16	1.07	0.25
90–150 US	23.1	0.60	3.10	0.32	11.70±.03	4.46±.15	1.37	5.134±.005	35.12±.33	0.74	0.13
60019,110	34.4	1.18	3.35	27.7	11.97±.01	3.15±.01	71.7	5.330±.005	9.69±.01	18.4	3.64
60255,93	30.2	19.5	38.6	18.2	12.09±.01	5.05±.01	204.	5.259±.003	2.54±.01	91.2	16.4
60275,56	17.2	2.04	6.21	14.8	12.02±.02	3.16±.02	18.3	5.324±.003	9.16±.03	14.3	2.53
61135,29	74.6	2.95	9.97	1.71	12.01±.02	3.28±.02	7.54	4.814±.003	17.92±.03	4.47	1.08
61175,206	30.0	17.6	41.4	13.8	12.22±.01	4.25±.01	141.	5.239±.005	4.58±.01	42.0	16.0
<20 FT	8.7	35.9	92.0	23.3	12.18±.01	3.63±.02	297.	5.089±.005	4.25±.01	122.	35.6
90–150 FT	18.6	11.0	21.4	6.83	11.82±.03	5.94±.11	60.3	5.118±.005	4.82±.01	34.1	9.75
61195,57	72.9	0.91	2.62	7.40	11.94±.01	3.22±.01	24.7	5.285±.005	10.97±.02	13.6	5.27
61295,47	34.1	17.4	40.8	14.1	11.71±.02	4.31±.02	98.3	4.976±.005	4.53±.08	58.7	20.8
61516,8	70.9	3.61	11.6	2.01	12.08±.01	3.27±.02	9.14	5.269±.005	15.48±.01	4.27	0.93
61525,9	23.1	7.50	20.0	7.03	11.43±.05	3.72±.02	47.3	5.103±.005	5.86±.24	30.5	5.39
61536,8	28.3	24.9	53.9	18.3	12.01±.01	4.31±.01	160.	5,184±.005	4.22±.01	75.5	24.0
63507,15	34.2	98.5	144.	53.8	12.48±.01	3.15±.01	292.	5.285±.005	0.737±.003	149.5	21.0
63588,6	77.8	1.27	4.15	0.65	11.92±.03	3.93±.04	3.69	5.153±.005	18.17±.02	2.45	0.82
63595,5	67.2	1.18	3.78	0.68	11.94±.02	3.81±.04	4.50	5.193±.005	16.63±.04	2.22	0.70
65095,78	72.3	0.032	28.8	0.0076	11.01±.44	16.19±.03	0.049	3.527±.008	479.±6	1.87	0.59
65715,11	52.5	6.33	18.5	3.11	12.00±.02	3.18±.03	9.97	5.264±.005	16.82±.03	12.6	3.22
66035,32	52.6	8.72	23.7	4.56	11.65±.02	3.09±.02	10.1	5.229±.005	14.54±.38	6.65	1.89
66036,10	78.1	4.14	13.9	2.28	12.06±.03	3.25±.03	10.2	5.247±.005	15.79±.03	4.48	1.21
66075,76	42.9	2.71	9.77	1.46	12.05±.03	3.33±.04	7.09	5.307±.005	17.83±.04	4.30	1.27
<20 FT	14.0	5.91	18.6	3.22	12.11±.03	3.23±.04	14.7	5.122±.005	13.85±.02	6.02	1.66
20–45 FT	18.4	2.96	10.40	1.90	11.88±.03	3.27±.04	9.55	5.286±.005	14.08±.01	19.3	0.91
45–90 FT	20.9	2.27	7.98	1.24	11.96±.02	3.55±.04	5.91	4.941±.005	16.74±.01	2.81	0.57
90–150 FT	25.1	1.04	5.59	0.58	11.87±.03	3.95±.09	2.77	5.030 ±.005	22.81±.01	1.47	0.3?

Data in several columns are to be multiplied by the power of ten indicated. Abundance uncertainties are estimated at +5% for He, Ne, Ar, and Xe and ±10% for Kr. Relative uncertainties for isotopic ratios are one sigma of the mean of multiple measurements of individual ratios plus one-half the applied blank corrections. Absolute isotopic ratios have an additional uncertainty of ±0.1%/mass unit.

primitive lunar soils that have not had extensive exposure at the lunar surface show considerably higher Ar ratios of about 4 to 8 [*Heymann*, 1975; *Lakatos et sl.*, 1973; *Bogard and Hirsch*, 1975]. The largest trapped ^{40}Ar/^{36}Ar ratios, however, have been observed in a few highland breccias and from glass spheres from the pyroclastic deposit exposed by Shorty crater at Apollo 17. Orange-black glasses from the 74001/2 core at Shorty crater gave ^{40}Ar/^{36}Ar of about 8 to 10. These "soils" have had only extremely short surface exposure (e.g., ^{36}Ar concentrations ~10^{-6} cm^3/g), and good arguments, largely independent of the measured ^{40}Ar/^{36}Ar, have been made that the solar gases were acquired about 3.7 b.y. (1 b.y. = 10^9 years) ago [*Eugster et al.*, 1980, 1981]. At least two Apollo 14 breccias (14301 and 14318) have trapped ^{40}Ar/^{36}Ar ratios of 10–14 [*Megrue*, 1973; *Reynolds et al.*, 1974; *Bernatowicz et al.*, 1980], although the time when these gases were acquired is not independently known. Thus there seems to be good evidence for the model that the implanted ^{40}Ar/^{36}Ar ratio has been about 1 in recent times but was much larger in early lunar history.

Figure 6 attempts to show the possible change in surface-implanted ^{40}Ar/^{36}Ar with time in a more quantitative manner. We assume that the ^{40}Ar/^{36}Ar in recent times is 1, which is the average value for several Apollo 16 soils with measured values between 0.7 and 1.5. The line in Figure 6 models the increase in ^{40}Ar/^{36}Ar back in time due to the increasing abundance of ^{40}K and represents a doubling of the ratio every 1.28 b.y. (the half-life of ^{40}K). The gas implantation times are approximately known for only a few samples, and these are compared with the model curve in the figure. The glasses from Apollo 17 Shorty crater are perhaps the most precise datum, and the gases were likely acquired at the time of their formation 3.7 b.y. ago [*Eugster et al.*, 1980, 1981]. The green glasses from Apollo 15 formed 3.38 b.y. ago and contain slightly lower ^{40}Ar/^{36}Ar of 5–6.3 [*Podosek and Huneke*, 1973; *Lakatos et al.*, 1973]. Another datum of lower precision than these glasses can be estimated from the Apollo 15 drill core soils. Soils below about 26-cm-depth probably were deposited between 450 and 900 m.y. ago [*Russ et al.*, 1972], and the largest trapped ^{40}Ar/^{36}Ar observed from analyses of grain size separates of these soils is 1.3–1.5 [*Pepin et al.*, 1974; *Bogard and Hirsch*, 1975]. These data points are roughly consistent with the model curve.

From the trend defined in Figure 6, the high trapped ^{40}Ar/^{36}Ar ratios in nine of these Apollo 16 regolith breccias (and in the two Apollo 14 breccias referenced above) suggests that they acquired their solar gases and excess ^{40}Ar approximately 4 b.y. ago. The trapped Ar ratios in the breccias are at least as large as those acquired by the orange/black glasses 3.7 b.y. ago. An upper limit to the time of solar irradiation would be set by the actual formation age of the rock components of the breccias. The only such ages available for these regolith breccias are a ^{39}Ar/^{40}Ar age of 3.9 b.y. for a clast in 61135 [*Schaeffer and Schaeffer*, 1977] and a ^{207}Pb/^{206}Pb age of 3.83 b.y. for 60075 [*Oberli et al.*, 1979]. Various model ages representing parent-daughter separation tend to be considerably higher. The extent to which ages determined for these breccias represent intense thermal metamorphism rather than rock formation, or the possibility that some fine-grained components may have partially escaped events that reset other portions of the breccias, are unknown.

The heavy isotopes of Xe in most of these regolith breccias

TABLE 9. FMR Data and Selected Isotopic Ratios for Apollo 16 Regolith Breccias

Breccia	FeO	Is/FeO	$^{40}Ar/^{36}Ar$	$^{136}Xe/^{130}Xe$	$^{129}Xe/^{130}Xe$
60016,165		0.5	12.2	2.51 ± .09	6.25 ± .33
60019,110		0.2	8.8	2.03 ± .03	6.48 ± .14
60255,93	0.27	17.	2.25	1.76 ± .01	6.21 ± .06
60275,56	0.52	4.	3.8	1.94 ± .04	6.38 ± .14
61135,29	0.17	0.5	12.5	2.40 ± .02	6.52 ± .06
61175,206	0.23	8.	4.25	1.79 ± .01	6.46 ± .03
61195,57	0.61	<0.1	9.3	1.97 ±.02	6.32 ± .06
61295,47	1.45	6.	4.1	1.81 ± .01	6.27 ± .03
61516,8	0.16	0.5	9.5	2.41 ± .04	6.46 ± .11
61525,9	0.19	3.	3.7	1.83 ± .01	6.40 ± .03
61536,8	0.29	9.	3.9	1.80 ± .01	6.42 ± .02
63507,15	0.76	48.	0.55	1.82 ± .01	6.27 ± .03
63588,6	0.25	0.4	3.3	2.26 ± .04	6.44 ± .12
63595,5	0.08	0.4	4.4	2.33 ± .09	6.56 ± .26
65095,78	1.14	<0.1	~0	2.19 ± .04	6.46 ± .13
65715,11	0.16	0.6	11.3	2.26 ± .18	6.49 ± .06
66035,32	0.24	0.5	10.5	2.30 ± .03	6.47 ± .08
66036,10	0.25	0.4	10.4	2.41 ± .03	6.47 ± .09
66075,76	0.61	0.5	11.7	2.29 ± .05	6.48 ± .15

FeO is equivalent weight percent metallic iron; I_s/FeO is the relative FMR maturity normalized to iron content; $^{40}Ar/^{36}Ar$ is the observed ratio corrected for an estimated component of ^{40}Ar from in situ decay of K; $^{136}Xe/^{130}Xe$ and $^{129}Xe/^{130}Xe$ are observed ratios with measurement uncertainties.

occur in relative abundances greater than solar wind Xe trapped in lunar soils. Except for small excesses at masses 124 and 126 due to cosmic ray effects, the relative proportions of Xe isotopic masses 124 through 130 in these breccias are similar to solar wind Xe trapped in lunar soils [*Eberhardt et al.*, 1972]. Xenon isotopes 131 through 136, however, show variable excesses, with the ^{136}Xe excess usually the largest (Table 9). These excesses in heavy Xe isotopes undoubtably result from fission and primarily occur in those breccias with low ^{36}Ar concentrations and high trapped $^{40}Ar/^{36}Ar$. Those five breccias with the highest ^{36}Ar do not contain this fission component. Figure 7 compares the amounts of excess fission Xe and trapped $^{40}Ar/^{36}Ar$ as a function of ^{36}Ar concentration for all 19 regolith breccias.

A few Apollo 14 and Apollo 16 breccias have been studied in detail to characterize the fission-produced Xe they contain [*Bernatowicz et al.*, 1978; *Swindle et al.*, 1985]. The fission Xe in these breccias generally occurs in far greater concentrations than can be accounted for by in situ decay of uranium, and the observed fission mass spectra match that for fission of extinct ^{244}Pu. Excess ^{129}Xe is present in a few breccias, presumably from the decay of extinct ^{129}I. The above investigators have shown that the excess Xe isotopes were not produced by radioactive decay within the sample, but rather that the excess Xe was produced elsewhere in the lunar crust and was adsorbed on grain surfaces before the breccia was lithified and was later "affixed" in some manner, possibly by shock effects. Variations in the relative amounts of excess ^{129}Xe and fission Xe in some samples suggest a time dependency in the acquisition of these Xe components [*Swindle et al.*, 1985]. This explanation implies that these breccias acquired this excess Xe very early in lunar history, possibly prior to 4 b.y. ago.

Bernatowicz et al. [1978] found excess, fission Xe in three Apollo 16 breccias, including two analyzed in this work (60019 and 60275), and in the two Apollo 14 breccias mentioned above with high trapped $^{40}Ar/^{36}Ar$. The concentrations of excess ^{136}Xe reported for the Apollo 16 breccias were 0.1–1.5 × 10^{-10} cm^3/g, which is similar to the excesses shown for 13 breccias in Figure 7. The total Xe and excess ^{136}Xe for breccias 60019 and 60275 reported by *Bernatowicz et al.* [1978] are similar to the concentrations found in our investigation. By contrast, the expected amounts of ^{136}Xe produced by in situ fission of uranium in these breccias is less than 0.05 × 10^{-10} cm^3/g [*Bernatowicz et al.*, 1978]. The whole rock analysis we made of each of these breccias does not permit an accurate determination of the fission mass spectrum of the excess Xe. However, the average mass spectrum of excess Xe in 12 of these breccias is 131/132/134/136 = 0.31/0.86/0.88 = 1.00 and is in approximate agreement with the expected mass spectrum from ^{244}Pu [*Bernatowicz et al.*, 1978]. A few of the breccias analyzed suggest possible small excesses in ^{129}Xe as well (Table 9), but the analytical uncertainties often overlap the apparent excess.

Both the high trapped $^{40}Ar/^{36}Ar$ ratios and excess fission Xe present in several of these Apollo 16 regolith breccias indicate that they acquired their noble gases, including solar wind gases, very early in lunar history, possibly as early as 4 b.y. ago. Thus it is informative to compare the composition of this ancient solar wind gas with much more recent gas trapped in lunar soils. We compared the $^4He/^{36}Ar$, $^{20}Ne/^{36}Ar$, $^{84}Kr/^{36}Ar$, and $^{132}Xe/^{36}Ar$ ratios for these regolith breccias with six submature Apollo 16 soils. The elemental ratios for these two data sets are essentially identical, except that a few of the breccias show some He loss. With only whole rock analyses, the isotopic composition of solar wind gases cannot be precisely determined. However, aside from the excess ^{40}Ar and fission Xe and small

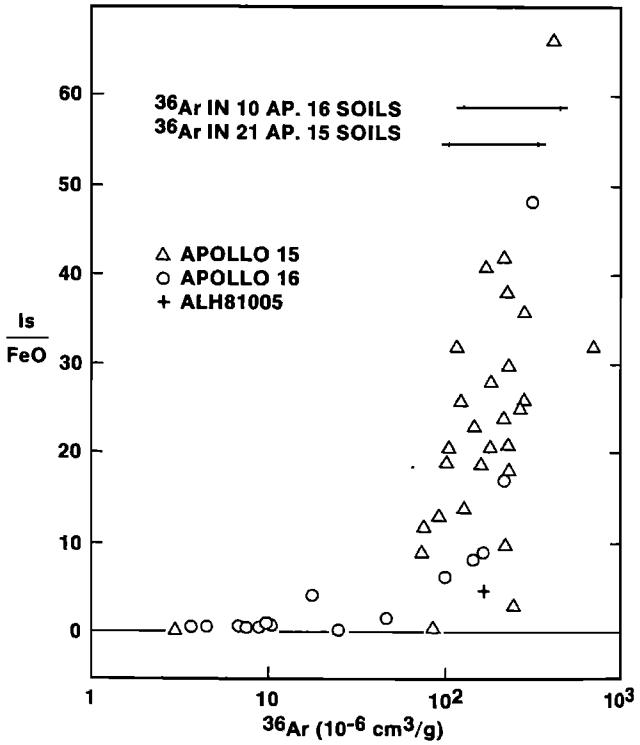

Fig. 5. The relationship between two surface maturity parameters, I_s/FeO (arbitrary units) and solar wind ^{36}Ar concentrations (10^{-6} cm^3/g), for Apollo 16 regolith breccias and Apollo 15 regolith breccias. The ranges of solar ^{36}Ar in 10 Apollo 16 soils and in 21 Apollo 15 soils are shown for comparison. Data for the lunar meteorite ALH81005 are also shown.

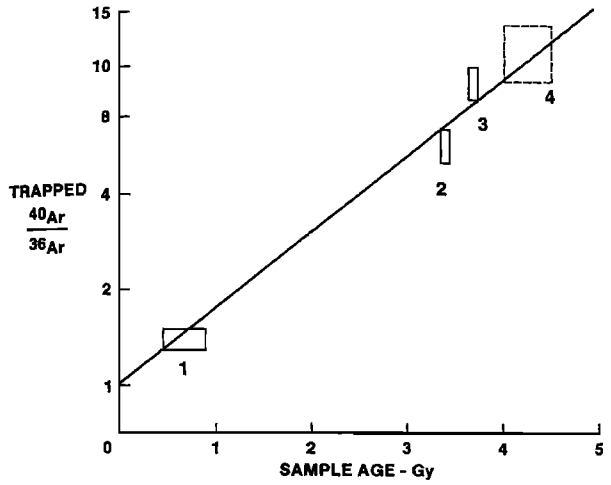

Fig. 6. Relationship between $^{40}Ar/^{36}Ar$ trapped in lunar regolith materials and the probable time of Ar implanation. The three solid data boxes represent regolith samples for which the Ar implanation times are most accurately known and are, from left to right, lower portions of the Apollo 15 deep drill core, Apollo 15 green glasses, and Apollo 17 orange/black glasses. The solid line represents the increase in $^{40}Ar/^{36}Ar$ back in time as predicted by the decay halflife of ^{40}K. The dotted box would be the position of nine of Apollo 16 regolith breccias on this trend given their trapped $^{40}Ar/^{36}Ar$ ratios of about 9–14.

cosmic ray components in some breccias, there is no obvious difference in the isotopic composition of Ne, Ar, Kr, and Xe in these breccias and in Apollo 16 lunar soils. The analyses of grain-size separates of breccias 60016 and 61175 support these conclusions. *Eugster et al.* [1980] also found no positive evidence for a difference between solar wind compositions trapped in orange/black glasses 3.7 b.y. ago and recent solar wind.

Comparison of Breccia and Soil Chemical Compositions

In this section we note the similarities and differences in composition between the soils and regolith breccias, and we point out some correlations between the chemical composition and surface maturity data. Chemical analyses by INAA were made on matrix-rich subsamples of 20–40 mg each that were selected to be representative of the breccia matrix, i.e., large clasts were avoided. In addition, M. M. Lindstrom and R. L. Korotev (unpublished data, 1985) separated clasts and matrix from separate samples allocated to L. A. Haskin of three of the breccias. The principle presentation of the results for the clasts will be made elsewhere (M. M. Lindstrom, unpublished data, 1986), but some of the data will be presented here. The matrix samples (one from 60016 and two each from 66035 and 66075) are chips and fines produced while removing the clasts. These samples weighing 25–118 mg, are designated M (matrix-rich chips) and F (fines) in Table 10.

INAA procedures used were similar to those of *Korotev* [1982] and *Korotev et al.* [1984]. The material and concentration value used as a standard for each element are listed in Table 10. Concentration values for Fe and the rare earth elements (REE) in the standard for these elements (i.e., NBS SRM 1633a, coal flyash) have been changed slightly from those of *Korotev et al.* [1984] as a result of restandardization against primary chemical standards. As controls, samples of nine Apollo 16 surface soils were analyzed with the regolith breccia samples. These data are also presented in Table 10. Concentrations of Al, Ti, Mg, V, and Mn were obtained for only 12 of the regolith breccia samples.

Scandium and Samarium

A useful tool for comparing the soil and regolith breccia compositions is a plot of an incompatible trace element (ITE), such as Sm, against Sc. Many authors have noted [e.g., *Bansal et al.*, 1972; *Nava and Philpotts*, 1973; *Taylor et al.*, 1973] that the concentrations of ITEs (those elements associated with KREEP) and "mafic" elements (those elements associated with mafic mineral phases, e.g., Mg, Fe, Sc, V, Cr, Mn) decrease with increasing Al concentration in Apollo 16 polymict materials. This occurs because the various anorthositic components at Apollo 16, which are the principle carriers of Al, are poor in ITEs and the principle carriers of Fe, Mg, and Sc, the impact melt rocks are rich in ITEs. (Some ITE-poor, mafic components may also be important.) On plots of ITEs or "mafic" elements against Al, Apollo 16 soils plot in the noritic or gabbroic anorthosite field between anorthosites ($Al_2O_3 > 31\%$) and the more mafic impact melt rocks of anorthositic gabbro composition ($Al_2O_3 < 25\%$). Although such plots are "standard," they are not particularly useful in discussing the regolith breccias.

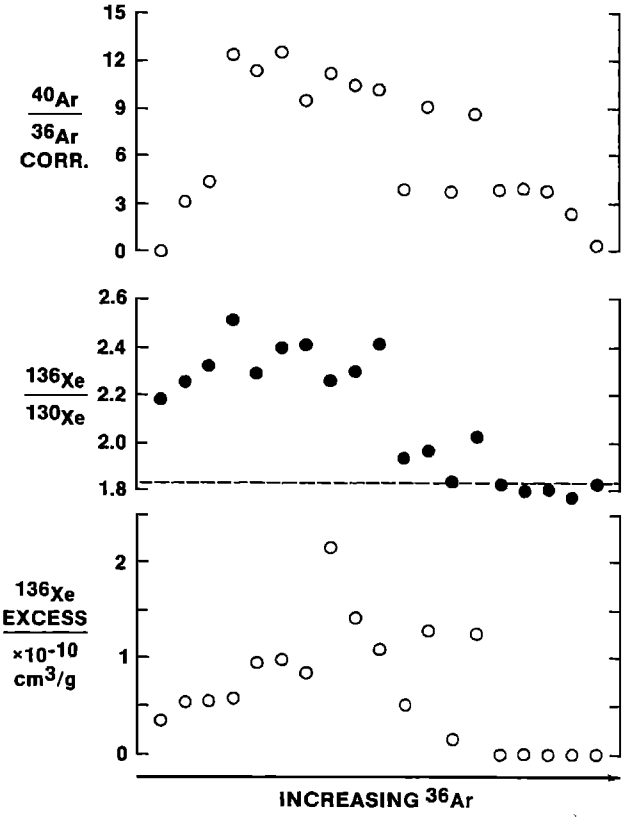

Fig. 7. Trapped $^{40}Ar/^{36}Ar$ (corrected for in situ decay of K), measured $^{136}Xe/^{130}Xe$, and excess ^{136}Xe (units 10^{-10} cm^3/g) plotted as a histogram of increasing ^{36}Ar concentration (in arbitrary units) for the Apollo 16 regolith breccias. The dotted line for $^{136}Xe/^{130}Xe$ shows the approximate value for solar wind implanted gas, and was used to calculate the excess, fission-produced ^{136}Xe concentrations. Those breccias with high trapped $^{40}Ar/^{36}Ar$ also have the largest ^{136}Xe excesses. Those breccias with the largest ^{36}Ar concentrations have trapped $^{40}Ar/^{36}Ar$ of ≤ 4 and show no excess ^{136}Xe.

More useful are plots of an ITE against a "mafic" element. Among rock types that are rich in one or both suites of elements, the proportion of "mafic" elements to ITEs is often different enough that plots of one against the other can be used to distinguish among different mafic and ITE-rich components. We choose Sm and Sc because both are precisely measured by INAA and many literature data are available for both elements. Compositional differences among the soils and breccias are more obvious on this plot than many others, hence a large part of the discussion below will be based on plots of Sm against Sc.

A disadvantage of using a two-element plot such as Sm versus Sc to infer mixing relationships is that a conclusion based on one such plot may be contradicted by another. For the purpose of testing assumed endmember mixing components, multielement models such as those of *Boynton et al.* [1975] or *Kempa et al.* [1980] must be used. These models can never uniquely prove that a particular set of assumed components represents the true endmember components of a mixture. They can, however, unambiguously show that the chosen set of components is inadequate to explain the composition. We choose not to discuss the data obtained here in terms of such models, although we have tested the conclusions reached below with the model of *Morris et al.* [1985]. In our experience, for systems with only a few important components many of the valid conclusions that can be drawn directly from the results of a multielement mixing model can also be drawn directly from the input compositional data, usually with a few key elements. The latter has the advantage of being conceptually simpler and avoiding the model dependence of the former. For presentation purposes, the Sm-Sc figures will be used to infer mixing relationships. The conclusions reached on the basis of these figures are supportable when other elements are also considered.

Figure 8 is a plot of Sm against Sc keyed according to sampling station for the regolith breccias and the surface soils. With few exceptions surface soils from a given sampling station are similar in composition to each other and usually overlap with soils from only one or two other stations. Compositions of the regolith breccias, however, neither cluster according to station nor correlate with soils from the station at which they were collected. This is in sharp contrast to what is observed at Apollo 15 where soils and regolith breccias from a given station are usually similar to each other in composition [*Korotev*, 1985]. This difference is probably related to differences in maturity of the regolith breccias at the two sites. Most of the Apollo 16 breccias are immature with respect to surface exposure whereas the Apollo 15 breccias are nearly as mature as the soils.

Other comparison can be made on Figure 8. None of the

TABLE 10. Chemical Composition of Apollo 16 Regolith Breccias and Some Representative Soils

Sample	I_s/FeO	Station	Mg' (%)	Al_2O_3 (%)	FeO (%)	MgO (%)	CaO (%)	TiO_2 (%)	Na_2O (%)	Sc	V	Cr
Soils												
60051	57.	LM	69	(28.5)	4.26	(5.05)	15.8	(0.44)	0.484	7.75		594
60601	85.	LM	70	(26.8)	5.28	(6.27)	15.9	(0.60)	0.455	9.18		720
61181	82.	1	67	(27.0)	5.40	(5.79)	15.6	(0.68)	0.482	9.54		761
61241	47.	1	68	(27.2)	4.95	(5.75)	16.1	(0.57)	0.495	9.06		689
63501	46.	3	68	(27.8)	4.47	(5.17)	15.7	(0.53)	0.505	8.05		588
65511	55.	5	69	(25.3)	5.82	(6.7)	15.9		0.491	10.56		820
65701	106.	5	67	(26.5)	5.55	(6.02)	15.8	(0.64)	0.468	10.05		772
66031	102.	6	70	(26.7)	5.66	(6.8)	15.7		0.452	9.75		758
66081	80.	6	68	(26.2)	5.73	(6.39)	15.6	(0.67)	0.459	10.29		782
Regolith Breccias												
60016,165	0.5	LM			4.47		15.7		0.469	6.72		545
60016,66 P					4.60		15.3		0.490	6.81		550
60019,110	0.2	LM			5.32		14.9		0.441	8.92		782
60255,93	17.	LM	70	26.4	5.32	6.6	15.6	0.61	0.469	9.50	21	739
60275,56	4.	LM	72	25.3	5.17	6.7	15.3	0.68	0.479	8.57	18	713
61135,29	0.5	1	72	29.4	3.31	4.5	16.7	0.54	0.542	4.96	<30	376
61175,206	8.	1			4.42		16.0		0.532	7.77		566
61195,57	<0.1	1			4.55		15.7		0.441	8.09		650
61295,47	6.	1			4.40		15.9		0.522	7.35		534
61516,8	0.5	1			4.22		15.9		0.509	6.22		484
61525,9	3.	1			5.25		15.1		t0.579	9.40		723
61536,8	9.	1	67	27.6	4.47	4.9	16.7	0.51	0.530	7.82	16	563
63507,15	48.	13	69	24.8	6.42	7.1	15.1	0.66	0.493	9.71	20	763
63588,6	0.4	13	72	28.9	3.64	4.95	16.0	0.37	0.491	5.65	14	449
63595,5	0.4	13	71	29.9	3.09	4.15	16.8	0.30	0.477	5.21	113	380
65095,78	<0.1	5	74	26.2	4.90	6.95	15.4	0.53	0.444	7.35	14	696
65715,11	0.6	5	71	27.0	4.24	5.45	15.7	0.48	0.492	7.25	14	555
66035,32	0.5	6	66	28.5	4.85	5.25	16.0	0.43	0.442	9.26	20	700
66035,27 F					5.03				0.554	8.54		692
66035,27 M					3.15				0.449	5.16		403
66036,10	0.4	6	73	27.8	4.30	6.10	15.8	0.47	0.506	6.83	20	540
66075,76	0.5	6	71	25.7	5.60	7.3	14.6	0.77	0.505	8.63	20	662
66075,14 F1					4.33		15.6		0.498	6.91		572
60075,14 F2					4.70		15.2		0.503	7.42		611
unc.(+/- s)				0.3-	0.03-	0.20-	0.3-	0.05-	.005-	0.05-	4-	5-
(range)				0.4	0.06	0.25	0.5	0.08	.015	0.10	5	8
BCR-1				13.2	12.1	3.1	7.5	2.62	3.29	32.3	355	10
1633a					12.07					38.6		
DTS-1				0.24	7.73	49.6		0.0		3.38	9	4245
AN-G				29.8	2.94	1.81	15.9	0.2	1.64	9.91	70	46

regolith breccia samples is as rich in Sc as the soils from Stations 5, 6, and 9. Aluminum concentrations in the high-Sc breccias and soils, however, are similar to each other (not shown). Several breccias have lower concentrations of Sc (and higher Al) than any surface soil. Many of the breccia samples have greater concentrations of Sm (and other ITEs) than any soils of similar Sc concentration and three have greater concentrations than any surface soil. Several others have Sm concentrations as low as only the North Ray crater soils at Station 11, but compared to the Station 11 soils the breccias have considerably lower concentrations of Sc. None of the regolith breccias plot in the field of the North Ray crater soils at Station 11 and no regolith breccias were collected at this station. No obvious correlation exists between Sm concentration and surface maturity, except that those breccias with the highest surface maturity have Sm concentrations very similar to the soils.

The comparison changes somewhat if the soils from the cores are included. Figure 9 plots all available data for Apollo 16 core samples. The anorthositic (low Sc) regolith breccia samples, for which there are no equivalents among the surface soils, do plot with the anorthositic soils from the 60009 drive tube. (Some importance differences in Fe and Mg between these breccias and soils, however, are discussed below.) None of the breccias is as low in Sc and Sm as the most anorthositic samples from 60009. A few of the breccia samples are still richer in ITEs than all soils except two atypical core samples. None of the breccias is similar in composition to those soils from 64001 that are rich in Sc (>12 ppm) as a result of a mare component. In summary, several breccia samples with very low surface maturities plot outside the range of soils and these trend toward higher Sm and/or lower Sc concentrations.

Before discussion of some possible reasons for these compositional differences between the soils and the regolith breccia, some other comparisons and observations must be made.

Chemical Heterogeneity

Figures 8–10 contain multiple analyses for some regolith breccia samples. Examination of Table 10 for samples for which multiple splits were analyzed (60016, 66035, and 66075) reveals that our efforts to obtain representative matrix samples were either not successful or that the concept of a "representative" matrix sample is not really valid. The data for the multiple sample splits scatter far more than do multiple splits of the same mass of <1-μm soils. (There are no data, however, to indicate whether this heterogeneity in the breccias is really any worse than would occur for soils of the same sample mass that had not been mixed and sorted by sieving and human handling.) The data for samples from 66035 and 66075 (including the data of *Boynton et al.* [1975], *Garg and Ehmann* [1976], and *Wänke*

Table 10. (continued)

Sample	Mn	Co	Ni	Sr	Zr	Cs	Ba	La	Ce	Nd	Sm	Eu
Soils												
60051	(310)	19.5	260	200	160	0.12	110	10.0	26.4	10	4.60	1.195
60601	(540)	31.6	453	183	160	0.14	139	12.1	31	19	5.77	1.19
61181		28.2	380	179	180	0.16	134	12.5	33	20	5.83	1.195
61241	(540)	21.2	282	186	140	0.15	124	11.4	30	17	5.36	1.205
63501	(480)	17.4	209	191	120	0.10	99	8.82	21.0	13	4.12	11235
65511	(610)	36.4	499	179	190	0.20	170	15.1	39	22	7.01	1.225
65701	(620)	29.0	420	210	200	0.18	160	14.4	38	19	6.65	1.24
66031	(582)	35.6	515	178	160	0.14	147	12.9	33	20	6.00	1.205
66081	(620)	32.2	461	178	160	0.16	153	14.3	36	21	6.77	1.205
Regolith Breccias												
60016,165		24.5	318	180	140	0.11	103	9.71	25.4	15	4.43	1.20
60016,66 P		30.3	445	170	150	0.16	150	12.6	32	22	5.68	1.235
60019,110		27.7	412	176	250	0.29	191	19.7	51	30	9.06	1.285
60255,93	530	33.3	436	191	170	0.17	143	12.4	32	20	5.72	1.195
60275,56	490	30.2	447	193	240	0.22	197	19.7	51	31	9.08	1.285
61135,29	340	13.2	146	211	85	0.10	78	6.41	16.7	10	2.93	1.22
61175,206		17.8	205	201	120	0.14	122	10.5	27.1	15	4.76	1.22
61195,57		18.9	248	176	140	0.10	103	9.23	24.2	14	4.24	1.12
61295,47		21.0	293	200	280	0.09	108	10.6	27.3	17	5.08	1.21
61516,8		22.7	382	212	150	0.11	114	10.4	27.6	17	4.76	1.245
61525,9		21.3	236	180	190	0.23	266	17.9	46	28	7.87	1.31
61536,8	530	21.6	260	186	160	0.09	114	10.0	26.6	15	4.77	1.20
63507,15	545	72.4	1020	201	140	0.14	146	12.7	32	20	5.90	1.265
63588,6	373	16.3	199	196	100	0.09	86	8.41	21.3	13	3.84	1.175
63595,5	340	10.8	114	191	90	0.08	64	5.46	14.2	8	2.50	1.125
65095,78	475	27.9	428	167	250	0.12	161	16.2	42	24	7.56	1.21
65715,11	430	20.8	283	189	170	0.19	133	13.7	35	22	6.32	1.245
66035,32	340	18.6	214	187	150	0.10	101	9.08	24.5	14	4.23	1.095
66035,27 F		21.5	310	205	200	0.23	200	17.5	44.9	28	7.84	1.465
66035,27 M		13.4	180	190	100	0.11	99	9.20	22.6	14	4.12	1.095
66036,10	455	19.1	241	181	120	0.12	113	10.2	26.2	15	4.72	1.15
66075,76	540	27.6	342	187	310	0.15	186	20.1	52	33	9.34	1.345
60075,14 F1		23.8	248	195	170	0.12	160	13.0	32.7	20	5.98	1.225
66075,14 F2		22.9	305	191	210	0.14	160	14.9	37.6	24	6.81	1.28
unc. (+/- s)	5-	0.2-	7-	10-	10-	0.01	3	0.05-	0.5-	2	0.03-	0.012-
range)	10	0.4	16	40	25	0.03	10	0.20	1.5	4	0.10	0.015
BCR-1	1410	37.6	<40	350	190	0.96	660	25.2	53	27	6.79	1.95
1633a		44.1		835	240	10.42	1320	79.1	168	76	16.8	3.58
DTS-1	940	139.1	2405									
AN-G		24.8	36	84	<50	0.05	33	2.17	4.8	2.4	0.72	0.36

TABLE 10. (continued)

Sample	Tb	Yb	Lu	Hf	Ta	Ir (ng/g)	Au (ng/g)	Th	U	Mass (mg)	Ref.
Soils											
60051	0.89	3.16	0.446	3.60	0.44	8.1	4.6	1.8	0.45	55.31	(a)
60601	1.04	3.91	0.567	4.28	0.51	16.1	7.5	22.05	0.62	49.93	(b)
61181	1.13	4.11	0.566	4.47	0.54	11.8	8.2	2.05	0.54	55.80	(c)
61241	0.93	3.71	0.510	4.03	0.49	11.3	4.3	2.10	0.52	58.54	(b)
63501	0.82	2.87	0.422	3.16	0.38	7.3	3.6	1.50	0.36	59.93	(d)
65511	1.30	4.94	0.706	5.47	0.66	14.3	8.5	2.49	0.66	50.98	(e)
65701	1.30	4.57	0.658	5.15	0.60	13.8	11.6	2.62	0.61	50.47	(b)
66031	1.10	4.19	0.597	4.72	0.55	14.3	11.6	2.37	0.56	54.51	(e)
66081	1.23	4.56	0.656	4.95	0.60	16.2	7.3	2.30	0.85	53.19	(b)
Regolith Breccias											
60016,165	0.82	3.03	0.430	3.30	0.40	7.6	4.6	1.64	0.42	55.00	
60016,66 P	1.02	4.03	0.553	4.34	0.52	10.1	19.	2.31	0.53	103.42	
60019,110	1.68	6.0	0.86	6.75	0.76	8.4	9.0	3.35	0.86	53.70	
60255,93	1.07	4.13	0.581	4.85	0.56	13.6	8.3	2.30	0.55	44.12	
60275,56	1.66	6.1	0.86	6.93	0.77	9.6	7.9	3.20	0.95	48.03	
61135,29	0.54	2.01	0.282	2.25	0.26	5.4	2.9	1.04	0.24	20.39	
61175,206	0.89	3.25	0.464	3.58	0.42	5.8	3.2	1.66	0.42	50.17	
61195,57	0.79	3.00	0.439	3.38	0.55	6.2	5.1	1.85	0.39	26.58	
61295,47	0.92	3.16	0.455	3.60	0.39	5.6	5.6	1.63	0.40	19.73	
61516,8	0.93	3.28	0.452	3.57	0.40	5.3	6.8	1.86	0.44	27.60	
61525,9	1.50	5.5	0.754	5.76	0.92	7.9	4.8	2.57	0.67	22.94	
61536,8	0.92	3.27	0.455	3.62	0.44	9.8	4.4	1.7	0.50	40.20	
63507,15	1.09	4.11	0.590	4.57	0.56	51.	17.	2.28	0.58	45.18	
63588,6	0.68	2.54	0.371	2.91	0.31	4.9	3.4	1.31	0.28	26.12	
63595,5	0.49	1.73	0.249	1.88	0.215	2.6	2.3	0.83	0.20	31.63	
65095,78	1.38	5.0	0.714	5.58	0.60	11.8	7.5	2.70	0.67	25.66	
65715,11	1.10	4.24	0.607	4.74	0.50	6.0	5.1	2.43	0.59	22.53	
66035,32	0.81	2.97	0.424	3.26	0.39	4.4	4.5	1.77	0.38	20.73	
66035,27 F	1.45	5.55	0.778	6.06	0.71	6.0	6.0	3.17	0.72	117.81	
66035,27 M	0.78	2.81	0.394	2.80	0.34	3.6	3.4	1.5	0.40	25.53	
66036,10	0.87	3.21	0.461	3.43	0.39	5.5	7.4	1.83	0.40	19.22	
66075,76	1.79	6.0	0.870	7.24	0.84	8.5	5.5	3.72	0.8	27.43	
66075,14 F1	1.10	4.18	0.576	4.38	0.49	5.2	12.7	2.08	0.53	85.64	
66075,14 F2	1.25	4.77	0.652	5.06	0.56	5.5	8.1	2.40	0.61	77.81	
unc.	0.02-	0.05-	0.004-	0.03-	0.02-	0.4-	0.5-	0.05-	0.05-		
range	0.05	0.15	0.016	0.10	0.03	0.7	1.0	0.15	0.20		
BCR-1	0.97	3.28	0.482	5.13	0.79	<2	<2	5.79	1.76	39.62	
1633a	2.38	7.50	1.075	7.29	1.93			24.0	10.3	51.83	
DTS-1										40.35	
AN-G	0.16	0.78	0.116	0.47	0.16			<0.1	<0.1	39.05	

I_s/FeO values from *Morris* [1978] (soils) and Table 9 (regolith breccias). Mg′ = mol % Mg/(Mg + Fe), corrected for meteoritic Fe and Mg via Ni, see text. Uncertainties are one standard deviation estimates of precision. Within the range listed, the smaller absolute uncertainties usually apply to lower concentrations, and conversely. Soil data are new for this work, except data for Al, Mg, Ti, and Mn in paremtheses are from: (*a*) = *Simkin et al.* [1973], (*b*) = *LSPET* [1972], (*c*) = *Taylor et al.* [1973], (*d*) = *Wänke et al.* [1975], and (*e*) = *Korotev* [1982]. Blanks indicate that the element was not determined. In the standards, the underlined value is that value against which all other values for the element were determined. Chemical standards were used for Ti, Mn, Ir, and Au.

et al., 1974, 1977] for the latter sample) nearly cover the range observed for all samples in Table 10. This problem is probably worse for some breccia samples than for others. It is important to keep in mind that the chemical analyses listed here are not necessarily representative of the matrix of the sample and that different sample splits were used for petrographic, noble gas, FMR, and bulk chemical analysis.

Siderophiles, Mg′, and Surface Maturity

Although the regolith breccias are not nearly as mature as the soils, the concentrations of siderophile elements are only slightly lower than those of mature Apollo 16 soils. Nickel concentrations, for example, average about 80% of the values found in typical soils. This indicates that the quantity of meteoritic material in the breccias is almost comparable to that in mature soils. However, the breccia with the highest solar gas concentrations and I_s/FeO value, 63507, has unusually high concentrations of siderophile elements. Its Ni and Ir concentrations are about 2.5 and 4 times greater than those of mature soils and are approximately equivalent to an 8% component of chondritic meteorite. This is large enough to make a significant effect on the concentration of several other elements. For example, the 24.8% Al_2O_3 and 7.1% MgO in this sample are, respectively, less and greater than the concentrations of these elements in any typical Apollo 16 soil. The FeO concentration is unusually high considering the concentrations of Mg and Sc. When the 8% of chondritic material is mathematically "unmixed" from 63507 to bring the Ni and Ir concentrations down to levels observed in the soils, the Al concentrations increases, Mg and Fe decrease, and the concentrations of all elements in 63507 become indistinguishable from those in typical Apollo 16 soils. Regolith breccias 63507 and 60255 are the most similar in compositon to typical soils and have the greatest values of I_s/

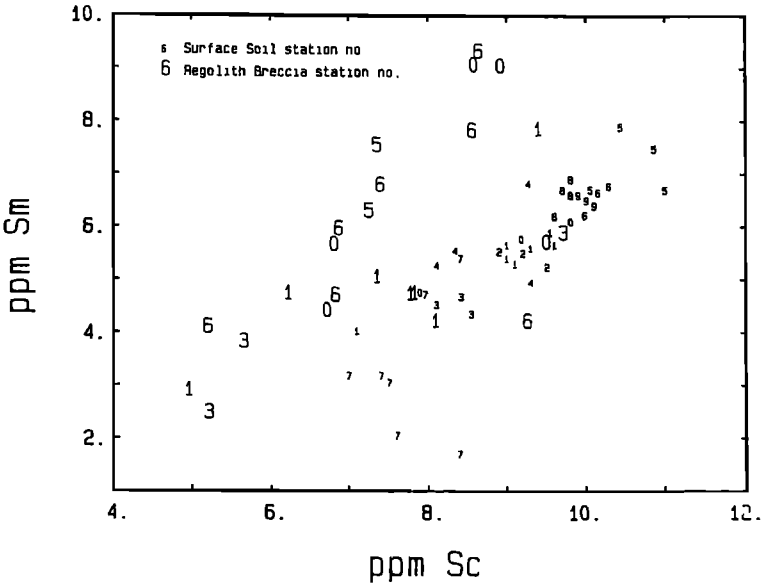

Fig. 8. Concentration of Sm and Sc in regolith breccias and surface soils, keyed to station number. Soil data from *Korotev* [1982].

FeO among the regolith breccias. In fact, all five sample with $I_s/FeO > 5$ (63507, 60255, 61536, 61175, 61295, in decreasing order of maturity) lie in the compositional field of the soils in Figure 10. All samples that lie outside the soil field have very little surface exposure.

Another important compositonal difference between the soils and some of the breccias is in their Mg/Fe ratio or Mg′ value (Mg′ = mol % Mg/(Mg + Fe)). The Mg′ value of mafic minerals is a useful discriminator among different rock types thought to be original materials of the lunar crust [e.g., *Warren and Wasson*, 1979; *Ryder*, 1979]. The Mg′ value calculated from bulk analysis of Fe and Mg is a weighted average of the Mg′ value of all the Fe-and Mg-bearing components in the rock or soil, including any meteorite component. Hence when comparing bulk values of Mg′ among samples with variable amounts of siderophile elements or when comparing bulk values obtained from mineral analysis, a correction for nonindigenous Fe and Mg must be made. To a good first approximation the correction can be made by reducing the Fe and Mg concentrations by a simple mass-balance calculation using the chondritic ratios of Fe/Ni and Mg/Ni and assuming a concentration of zero for the indigenous lunar Ni component. (The results are trivally different if, for example, a value of 100 ppm indigenous Ni is assumed.) This is the same correction procedure used by *Morris et al.* [1985] and discussed in more detail by *Korotev et al.* [1984]. (In principle, Ir or Au could be used instead of Ni for this correction. Analytical precision for Ir and Au is not as great as for Ni, however, and the data of *Korotev et al.* [1984] show that Ni correlates better with the excess Fe and Co than do Ir and Au. Iridium and, to a lesser extent,

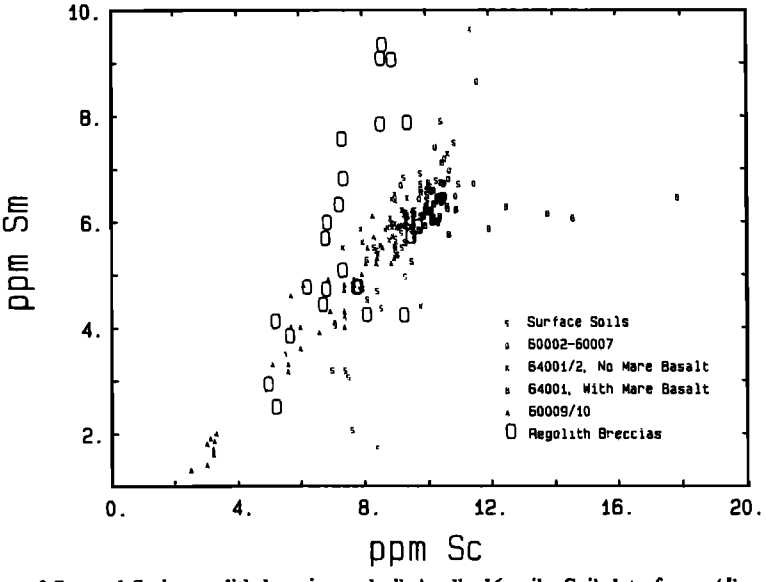

Fig. 9. Concentration of Sm and Sc in regolith breccias and all Apollo 16 soils. Soil data from *Ali and Ehmann* [1976, 1977]; *Blanchard et al.* [1976]; *Korotev* [1982, 1983]; and *Korotev et al.* [1984].

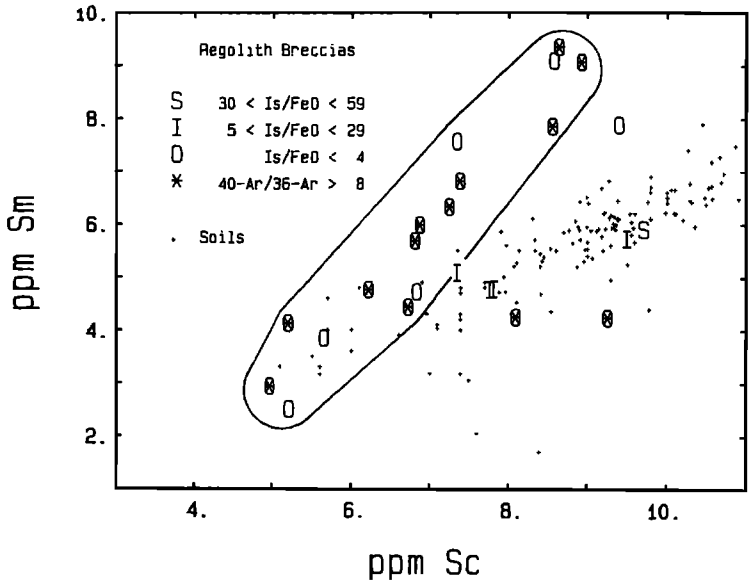

Fig. 10. Concentration of Sm and Sc in Apollo 16 regolith breccias, keyed according to surface maturity, and comparison to Apollo 16 soils. The soil data are the same as in Figure 9, except that some core soils that plot off the figure are not included. The enclosed diagonal field, which is distinctly different than the field of the soils, includes all regolith breccias with Mg′ values >70. All of these breccias are immature and most have high $^{40}Ar/^{36}Ar$ values. Those regolith breccias lying outside the diagonal field are usually more mature, have lower Mg′ values and are compositionally more similar to the soils. Those samples plotting inside the diagonal field are the "magnesian" and "ancient" subset discussed in the text.

Au concentrations also are quite variable among small subsplits of the Allende meteorite reference sample that have virtually identical Ni concentrations (R. L. Korotev, unpublished data, 1985), suggesting that Ir is not as useful as is Ni for the purpose of correcting for the meteorite component.)

Figure 11 is a histogram of meteorite-corrected Mg′ values for soils and regolith breccias. Most of the regolith breccias have a greater value of Mg′ than do the soils. Typical Mg′ values for the breccias are 71 whereas those for the soils are 68. This indicates that there is a subtle but distinct difference in the population of Fe- and Mg-bearing minerals composing the high-Mg′ breccias compared to those of the soils. Some regolith breccias, however, have lower Mg′ values, in the range for soils. This dichotomy extends to other parameters. All the breccias with Mg′ < 71 plot in the field for the soils on the Sm versus Sc plot of Figure 10. Magnesium concentrations have been measured on four of the samples with Is/FeO > 5 and all four of these are among the low-Mg′ samples. All of the samples with Mg′ > 70 plot in the diagonal field, which is distinctly different from the trend of the soils in Figure 10. Magnesium concentrations were not measured on all of these samples, but for a few of them literature analyses are also available and the trend holds. All of the samples plotting in this diagonal field of magnesian samples have low surface maturities ($I_s/FeO < 5$). Also, samples from eight of the nine breccias with $^{40}Ar/^{36}Ar$ ratios exceeding 8 are magnesian. (Sample 61195 is the exception. The data of *Wänke et al.* [1975] yield a Mg′ value of 67, consistent with other samples that plot to the high Sc side of the diagonal trend.) One of the three 66035 samples, 66035,32, also plots outside the field of magnesian samples, but the two larger samples plot inside. (Sample 66035,32 is clearly an unusual, mafic composition with the lowest value of Mg′ measured here, 66. It may not be representative of the whole sample.)

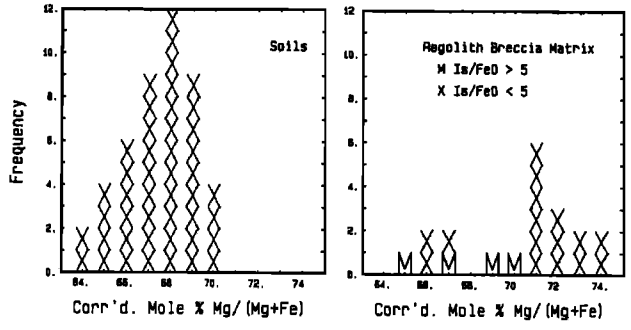

Fig. 11. Histogram of Mg′ (corrected for meteoritic Fe and Mg—see text) for regolith breccias and typical Apollo 16 soils.

In summary, the most mature regolith breccias are also the most similar to the typical soils in composition. However, three-quarters of the samples are distinctly different than the soils in having higher values of Mg′ and plotting outside the field of the soils on the Sm versus Sc plot. These have little surface exposure. The sample with no solar wind gas, 65095, is the most magnesian among the 12 samples for which Mg′ was determined. In the following discussion the "magnesian" subset of regolith breccias will refer to those samples plotting in the diagonal trend in Figure 10 and 12, specifically, 60016, 60019, 60275, 61135, 61516, 63588, 63595, 95095, 65715, 66035 (excluding split 66035,29), 66036, and 66075.

Chemical Components of the Regolith Breccias

What components can account for the difference between the compositions of the typical soils and the more magnesian subset of regolith breccias? The first step toward answering this question is to explain the diagonal trend of the magnesian regolith breccias in Figures 10 and 12. The trend is most easily

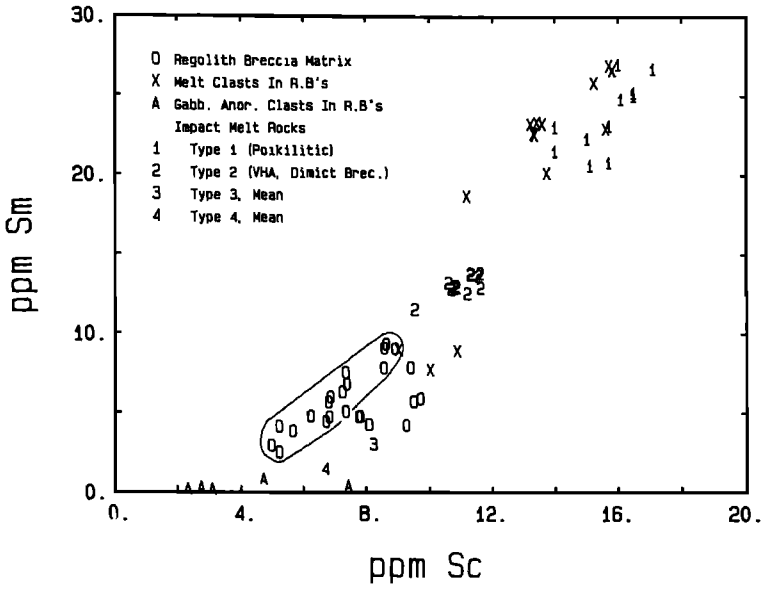

Fig. 12. Concentration of Sm and Sc in regolith breccias compared with Apollo 16 melt rocks. The regolith breccia data are the same as in Figures 8–10. The diagonal field of magnesian breccias of Figure 10 is also shown here. The "A" and "X" points represent analyses of clasts removed from three magnesian regolith breccias, 60016, 66035, and 66075 (data primarily from M. Lindstrom, unpublished data, 1985, and also two analyses of 66016 from *Wänke et al.* [1975] and two analyses of 66035 from *Warren and Wasson* [1978, 1979]). Data on type-2 melt rocks from *McKinley et al.* [1984] and *James et al.* [1984]. Data on remaining melt rocks from various sources referenced in *Ryder and Norman* [1980].

explained as a mixing line between a low-Sc, low-Sm component and high-Sc, high-Sm component. It represents the same mixing relationship seen in Figure 2 (percent FeO versus ANT). The low-Sc, low-Sm (ANT suite) component is a material of gabbroic or noritic anorthosite composition with 2–5 ppm Sc, <2 ppm Sm, and an Mg′ value of 71–72. Among possible rock types several candidates can be eliminated. The low-Sc, low-Sm component cannot be "pure" (35% Al_2O_3) anorthosite because the samples in the diagonal field in Figure 12 extrapolate to 30–31% Al_2O_3 on a plot of Sm versus Al_2O_3 (not shown). This component is not equivalent to either anorthosite mixed with soil, such as found in the most anorthositic samples from the 60009 core, or anorthosite mixed with impact melt rock, such as would occur if the dimict breccias were comminuted. The implied composition is also not that of the type-3 and type-4 impact melts of *McKinley et al.* [1984]. Both of these have greater concentrations of Sc than that required by the trend in Figure 12. The feldspathic fragmental breccias associated with North Ray crater have appropriately low ITE concentrations but have higher Sc concentrations and lower Mg′ values [*Lindstrom and Salpas*, 1981, 1983] than the low-Sc, low-Sm component required here. None of the compositions discussed above is adequate alone as the implied ANT suite component.

Some information about the nature of the low-Sc, low-Sm component might be obtained from clasts of this composition found in the breccias. Compositional data are available for four clasts of noritic or gabbroic anorthosite from regolith breccias plotting along the diagonal trend of Figure 12 (two analyses of a clast from 66035 [*Warren and Wasson*, 1978, 1979], one from 60016 [*Wänke et al.*, 1975], and one each from 66035 and 66075 (M. M. Lindstrom, unpublished data, 1985; see analytical methods above). All four clasts plot near the low-Sm extension of the apparent mixing trend in the Sm versus Sc plot (Figure 12). Alumina concentrations in the two samples for which there are data are 29.5% and 30–31%, in the required range calculated above. The feature that distinguishes these clasts from the other gabbroic and anorthositic norite materials described above is their low concentrations of ITEs compared to polymict materials of similar mafic/felsic ratio and low Sc concentrations. The clast analyzed by *Warren and Wasson* [1978, 1979] is described as a granulite and all four clasts are similar to, but slightly more felsic than, the magnesian granulites discussed by *Lindstrom and Lindstrom* [1986]. The compositional data suggest therefore that if the low-Sc, low-Sm component of the diagonal trend in Figure 10 and 12 is dominated by a single rock type, the rock type is most likely a noritic or gabbroic anorthosite such as the granulitic breccias that Lindstrom and Lindstrom argue to represent an important part of the ancient lunar crust. However, the Cr/Sc ratios for the magnesian granulitic brecias may be too high (~120, *Lindstrom and Lindstrom* [1976] for them to be the low-Sc, low-Sm component. Alternatively, this component may not be a single rock type but a mixture of several rock types with a noritic anorthosite bulk composition. One possibility is that the diagonal trend results because the various samples are composed of a relatively fine-grained matrix of mixed material of noritic anorthosite composition and variable amounts of a component, perhaps coarser-grained, with high Sc and Sm concentrations.

The common high-Sc, high-Sm rocks at Apollo 16 are the mafic impact melt breccias. There are two types of high-Sc, high-Sm melt rock (see review of *Spudis* [1984] and the data of *McKinley et al.* [1984]). The type-2 melt rock (alias VHA basalt or aluminous LKFM melt rock) is common at the site and is the melt phase in the dimict breccias. The type 1 melt rock (alias poikilitic melt rock, Apollo 16 KREEP, or mafic

LKFM melt rock) is richer in Sc and Sm than the type-2 melt rocks and is regarded by *Spudis* [1984] as rarer than the type-2 melt rock.

Figure 12 shows the field for regolith breccias with data for samples of the two types of high-Sc, high-Sm melt rocks plotted. Also plotted on Figure 12 are data for 14 clasts of melt rock separated from three of the magnesian regolith breccias. These include four clasts from 66035, six from 66075, two from 60016 (M. M. Lindstrom, unpublished data, 1985), and two additional clasts from 60016 [*Wänke et al.*, 1975]. Based on the concentrations of all elements, eleven of the clasts are type-1 and the remaining three are type-2 melt rocks. The latter clasts, which are all from 66035, are more similar in composition to samples 60335, 61016, and 64455 (not plotted) than they are to the melt portion of the dimict breccias, i.e., they are less mafic and less rich in ITEs. Both type-1 and type-2 melt rocks plot on or near the extension of the diagonal trend in Figure 12. Hence if the trend is primarily the result of varying amounts of a single type of melt rock, then it should be possible to identify the predominant melt rock. We do not know whether there is any significance to the predominance of type-1 melt clasts among those selected for analysis. It may be, for example, that the type-1 clasts are larger or for some other reason are more easily extracted from the breccias.

In order to determine whether type-1 or type-2 causes the mixing trend observed in Figure 12, we have done multielement mixing calculations such as those described by *Morris et al.* [1986]. For these calculations the mean composition of the three samples with highest Sc and Sm concentrations was modeled as a mixture of the mean composition of the three samples with the lowest Sc and Sm concentrations and various melt-rock compositions. The best fit with a single melt rock component is with about 30–40% type-1 melt rock; however, this fit is not really sufficient to explain the major-element composition of the high Sc and Sm samples. Better fits are obtained when both type-1 and type-2 melt rocks are included, but even these do not adequately account for both Fe and Mg. Magnesium values for the regolith breccias do not change systematically from the samples with low concentrations of Fe, Mg, Sc, and Sm to those with high concentrations of these elements, despite a 60% increase in Fe and Mg concentration. This implies that the trend is the result of a simple two-component mix and that both components have approximately the same Mg/Fe ratio. The type-1 melt rocks (meteorite corrected) have most nearly the same Mg value as the regolith breccias, again suggesting that the type-1 melt rocks are the dominant high-Sc, high-Sm causing the trend in Figure 12. Type-2 melt rocks have higher Mg values, typically 75–79 (meteorite corrected). Because they have lower concentrations of Fe, Mg, Sc, and Sm, a larger proportion of this type of melt is required in the mixtures and Mg value of the overall mixture is raised above the range of 71–74 observed in the regolith breccias. Hence if the type-2 melt rocks are also an important component of the magnesian regolith breccias, then the high-Sc, high-Sm component implied by the apparent mixing line in Figure 12 must itself be a fortuitous mixture of components that includes both type-1 and type-2 melt rocks as well as a more ferroan component that effectively cancels the high Mg value of the type-2 melt rocks. We conclude that although type-2 melt rocks, which are regarded as Nectaris ejecta [*Spudis*, 1984], are components of the ancient (magnesian) regolith breccias, most of the variation in composition among them is caused by variation in the amount of type-1 (Apollo 16 KREEP) melt rocks, which are thought to be ejecta from the Imbrium event [*Spudis*, 1984].

It would be interesting to test whether the present soils contain a different proportion of type-1 to type-2 melt rocks than do the magnesian regolith breccias. This test is difficult to make because the present soils contain at least one component not present or important in these breccias. Typical Apollo 16 soils are richer in Sc than the regolith breccias (Figure 10). This enrichment is even apparent, but less obvious, in plots of Al and Fe (meteorite corrected) versus Sc (not shown). It is likely, but not necessary, that the Sc-rich component present in soils (and soil-like regolith breccias) is a ferroan component and is the cause of the lower Mg′ value for the soils (Figure 10). It is also likely that it is relatively poor in ITEs because high-Sc soils are not as ITE-rich as are the most Sc-rich regolith breccias. This analysis indicates that if the differences between the compositions of the present soils (and soil-like regolith breccias) and the ancient, magnesian regolith breccias are caused by a single additional component in the soil, then the component is relatively mafic, ferroan (Mg′ < 68), not rich in ITEs, and well mixed in the soils. Several possibilities exist and these have been discussed by *Korotev* [1981, 1982, 1983]. Ferroan anorthositic norite, such as 67215 [*Lindstrom and Salpas*, 1983], meets the requirements and is a useful component in mixing models [e.g., *Morris et al.*, 1986??], but it is a far rarer rock type among large rock samples than is implied by its calculated concentrations in such models. The suite of magnesian gabbronorites [*James and Flohr*, 1983; *Lindstrom*, 1984] also contains samples that might cause the compositional differences, but these are unusual, evolved compositions that may be petrologically difficult to explain in the quantities required. Another possibility is mare basalt. The discovery of significant quantities of mare material in the 64001/2 core [*Korotev et al.*, 1984] makes the possibility more likely that mare basalt is a cryptic component in other Apollo 16 soils. The 3-ppm enrichment of Sc in typical Apollo 16 soils compared to magnesian regolith breccias with the same Sm concentration (Figure 10) would require addition of about 4% mare basalt. However, such a large enrichment is not consistent with other chemical data. First, Ti concentrations in the soils are the same as in the breccias. Second, the FeO-Sc data for the soils and the magnesian regolith breccias are colinear as shown in Figure 13. Their FeO/Sc ratios are 5000 ± 500 and 5200 ± 400, respectively. The corresponding ratio for mare basalts is approximately 2500. This large difference in FeO/Sc ratios means that an addition of 4% mare basalt to the magnesian breccias would pull them significantly off of their original trend so that the resulting soils would no longer be colinear with the original breccias. Only an addition of a component with similar FeO/Sc ratio would maintain the observed colinear relationship between the regolith breccias and the soils shown in Figure 13. The FeO/Sc ratio for 67215 is approximately 4500 and within the range observed for the regolith breccias and soils. Thus the addition of material of this composition to the magnesian breccias would account for the observed trends on Figure 13. However, as discussed above, the rarity of 67215-type material in the Apollo 16 rock collection makes it difficult to attribute to it the significant chemical differences that we see between most regolith breccias and the soils. Until the Sc-rich, ferroan components(s) of the present soils is positively identified, the chemical data for the soils cannot be used to

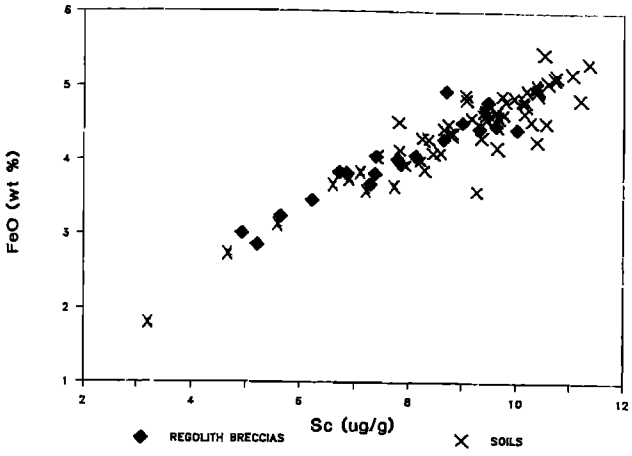

Fig. 13. Plot of FeO versus Sc abundances (meteorite-free basis) for regolith breccias and soils from Apollo 16. Soil data from *Ali and Ehmann* [1976, 1977], *Blanchard et al.* [1976], and *Korotev et al.* [1982, 1984].

infer whether type-1 or type-2 impact melt rocks are more prevalent in the soils and whether there is any significant change from the distribution found in the regolith breccias.

DISCUSSION

As a prelude to discussing the possible origin of the Apollo 16 regolith breccias and their relationship to other lunar materials, it is worthwhile to summarize some of the more pertinent observations made in the preceding sections. The porosities of Apollo 16 regolith breccias are variable but always less than lunar soils, are strongly correlated with shock features, and are undoubtedly determined by the breccia-forming event. Lithic fragments make up the majority of breccia grains larger than 500 μm. For grains smaller than 500 μm, the most abundant phases tend to be (1) mineral grains, mainly plagioclase, followed by (2) lithic fragments including crystalline and breccia varieties, the latter rarely being derived from regolith or fragmental breccias, followed by (3) clast-laden or quench-crystallized glasses. Agglutinates compose a small fraction of the grains in some of these breccias but are essentially absent in others. The ropy and homogeneous glasses are not proportional to the agglutinitic glasses, and ropy and homogeneous glasses probably formed by melt processes associated with large-scale impacts rather than those associated with micrometeorite working of surface materials. The lithic crystalline fragments (mainly anorthosites) vary in abundance relative to the melt matrix fragments, and a correlation between the ratio of these components and the FeO content suggests that these two rock types may be endmember components of a mixing trend.

Chemical compositions of regolith breccias neither cluster according to their collection station nor correlate with soils from the same station, which is in sharp contrast to Apollo 15 soils and regolith breccias, for example. Compared to the surface soils most breccias have lower concentrations of mafic elements, such as Sc, and higher concentrations of incompatible trace elements (ITEs). The breccias also tend to have slightly greater values of Mg′ than do soils, suggesting a subtle difference in the population of Mg- and Fe-bearing minerals. Three quarters of the breccias fall outside the compositional field for the soils defined by Sm, Sc, and Mg′. The breccias compositonally least like the soils are those with the lowest surface maturity, whereas those breccias with the largest regolith component are compositionally most like surface soils. Concentrations of siderophile elements (e.g., Ni) are nearly as high in the breccias as in mature soils, indicating that the meteoritic component in the breccias is nearly as great as in the soils.

The chemical and petrological data suggest that material of gabbroic or noritic anorthosite composition may be the low-mafic, low-ITE component in the Apollo 16 regolith breccias. The breccias contain essentially no chemical or petrological evidence of any mare basalt component. Samples with greater concentrations of Fe, Mg, Sc, and ITEs result from greater proportions of melt rock components. Although both type-2 (VHA basalt) and type-1 (poikilitic or LKFM melt) occur, the latter appears to be the predominant type. Compositional data for several melt rock clasts separated from several of these breccias seem to confirm this conclusion.

With the assumption that the chemical components of the regolith breccias are also important components of the present soils, then the soils contain at least one, well-mixed component in considerably greater proportion than is found in the regolith breccias. If it is a single component, it is relatively rich in Sc and Fe but poor in ITEs and ferroan (Mg′ < 70). If this component is from the highlands, such as ferroan anorthositic norite 67125, then an approximate 10% addition to the regolith breccias is necessary to explain the soil compositions. If this component is mare basalt, then no more than 4% is required to account for the Sc enrichment in the soils over that of the regolith breccias of similar general composition. However, an addition of mare basalt would have shifted the colinear trend observed on an FeO/Sc plot for regolith breccias and soils; this shift is not detectable.

Three of the regolith breccias were disaggregated by ultrasonic and freeze-thaw techniques, and the grain sizes produced were compared to breccia thin sections and to soils. Concentrations of solar wind-implanted gases is greater in the finer grain sizes than the coarser sizes, which confirms that the disaggregated grains roughly mimic the grain-size distribution at the time of irradiation before compaction. The disaggregated breccias have log normal grain-size distributions comparable to typical mature soils, having relatively low standard deviations and a lack of bimodality. The relative abundances of mineral grains, lithic and breccia fragments, and ropy and homogeneous glass in the disaggregated grains are quite similar to their relative abundances determined from thin sections, and suggest that the breccias disaggregated by both techniques were not appreciably changed in their petrologic components. The analyzed grain-size distributions should thus be similar to the grain-size distributions of the original fragmental material from which the breccias were made. The overall modal composition of disaggregated 60016 is similar to typical soils in spite of the fact that it contains only minimal evidence of surface maturation.

Apollo 16 regolith breccias have much lower concentrations of surface maturation parameters such as solar wind gases, agglutinates, and I_s/FeO compared to typical lunar soils and other regolith breccias. Many (but not all) of those breccias with low solar gases and I_s/FeO also tend to have very low cosmic ray irradiation times, suggesting that their integrated exposure at both the lunar surface and in the uppermost meter of the regolith has been very low. Data on disaggregated breccias suggest that the mature component is distributed across grain sizes and indicates a very short irradiation time of the breccia components prior to compaction. Nine of the breccias with low

solar gases have unusually high ratios of about 8–12 for trapped $^{40}Ar/^{36}Ar$. This Ar ratio at the lunar surface is widely believed to have substantially decreased over the age of the moon. Trapped $^{40}Ar/^{36}Ar$ ratios of 8–12 are as large as or larger than those seen in any other lunar materials. Measured ratios in a few lunar samples for which the irradiation time is approximately known suggest that the solar wind irradiation of these breccias occurred approximately 4×10^9 years ago. Those breccias with high trapped Ar ratios also have excess fission ^{136}Xe probably due to the decay of ^{244}Pu and acquired by the breccia very early in lunar history in a manner analogous to a few Apollo 14 breccias that also contain similar amounts of Xe from Pu fission.

Origin of Apollo 16 Regolith Breccias

Several observations indicate that most of the Apollo 16 regolith breccias were not formed by compaction of local soils. Among these are (1) the chemical differences between breccias and soils in both incompatible trace elements (e.g., Sm)- and mafic-related elements (e.g., Sc) and the evidence that the soils contain an iron-enriched component not present in the breccias, (2) the enhanced abundance of ropy and quenched glasses over agglutinitic glasses in the breccias compared to soils, (3) the nearly complete absence of fragments of regolith and fragmental breccias, (4) the much lower surface maturity of most of the breccias evidenced by their lower concentrations of solar gases, I_s/FeO, and agglutinates, and (5) the evidence from high trapped $^{40}Ar/^{36}Ar$ ratios and the presence of excess fission Xe that the solar wind contained in many of these breccias was acquired at a much earlier time than solar gases in the soils. On the other hand, the grain-size distributions of these Apollo 16 reoglith breccias are similar to mature soils and indicate that the breccias were formed from well-comminuted, fine-grained material. Furthermore, the high siderophile element content of the breccias suggests a meteoritic component nearly as large as typical Apollo 16 soils. The breccia material does not resemble typical immature soils in its grain-size distribution; it is much finer grained, better sorted, and lacks typical bimodal distributions. A few of the above observations, i.e., the low surface maturity, the high ratio of ropy and homogeneous glasses to agglutinitic glass, and the rarity of fragments of regolith or fragmental breccias, suggest that the Apollo 16 regolith breccias were in general not formed by multigenerational regolith processes such as occur in the upper portions of the present-day lunar regolith.

The fragmental material that formed the Apollo 16 regolith breccias may include an important, previously unrecognized regolith component. Many of these regolith breccias formed from well-comminuted, well-sorted material with appreciable abundances of nonagglutinitic glass but very low surface maturity. Such material is essentially unknown among lunar soils, where the degree of fragmentation correlates with agglutinitic glass and surface maturity. The high abundance of ropy and homogeneous glasses compared to agglutinitic glass suggests a different glass-forming process than presently occurs for lunar soils; the presence of excess ^{40}Ar and fission Xe suggests that solar irradiation and probably the breccia-forming events occurred very early in lunar history. This circumstance appears to be in contrast with the case for Apollo 15 regolith breccias, which have many more similarities with local soils (paper in preparation). The Apollo 16 regolith breccias cannot be made by simply mixing a small amount of mature soil with a large amount of freshly comminuted ejecta; this mixing would not allow for the relatively high abundance of ropy and homogeneous glasses because such glasses are dominated by agglutinates in typical mature soils.

We suggest that the Apollo 16 regolith breccias formed as a consequence of large cratering events during the early period of major bombardment of the moon. During this period the number of large cratering events were greatly enhanced and can be expected to have caused appreciable fragmentation and deep mixing of material. The homogeneous and ropy glasses would thereby be the consequence of melting within large craters. The low abundance of agglutinitic glass and other surface maturity parameters would reflect much shorter residence times at the lunar surface and a ratio of large impacts to small impacts significantly higher than the present-day ratio. The chemical differences between regolith breccias and local soils would thereby reflect addition of other components to the soils over the appreciable time period after breccia formation. The high siderophile element content of the breccias, however, would represent a meteoritic component acquired during the major bombardment period. We speculated that these regolith breccias may be part of the early megaregolith, either the upper zone of the megaregolith, the fine-grained part of the size distribution from deeper zones, or, some combination. Conceivably, the regolith breccias could be representative of the bulk of the entire megaregolith. If so, the relatively high proportion of fine-grained material in these regolith breccias is unexpected in terms of most concepts of megaregoliths.

The relationship between the Apollo 16 regolith breccias and the feldspathic fragmental breccias remains unclear. The feldspathic fragmental breccias differ slightly in composition having somewhat lower abundances of ITEs. Feldspathic fragmental breccias also appear to be relatively fine-grained but apparently contain no identifiable regolith component, so it is unlikely that they are derived from Apollo 16 regolith breccias. However, the reverse case cannot be ruled out. One possibility is that the two breccia types are contemporaneous and represent different zones of a megaregolith.

Whether the regolith material in the ancient Apollo 16 regolith breccias developed before or after the Imbrium and Nectaris events or possibly between also remains uncertain. As discussed earlier, dates as young as 3.8–3.9 b.y. have been determined for a few clasts in these breccias. This would make the regolith breccias as young as or younger than the basin-forming events. However, one possibility is that the regolith material in these breccias acquired its maturity before the Imbrium and Nectaris events and was mixed with younger rocks during or after these events but before being incorporated into a breccia.

Relationship to Meteorite Breccias

Simon et al. [1984] discuss the similarities of howardites and polymict eucrites to the Apollo 11 regolith that they have studied in detail. They suggest that lunar regolith breccias are better analogs than lunar soils for these meteorite breccias. We agree and suggest that the Apollo 16 regolith breccias are even better analogs because of the extremely low maturity and extremely low concentration of fused soil components in both Apollo 16 regolith breccias and meteoritic breccias. The Apollo 16 regolith breccias contain as much as 68% mineral fragments, much higher than typical soils, higher than Apollo 11 regolith breccias, and much closer to the howardites and polymict eucrites discussed in *Simon et al.* [1984], which contain about 90% mineral

fragments. As discussed above, our interpretation of the Apollo 16 regolith breccias is that they were formed during a period when large impacts were much more frequent and the ratio of large impacts to micrometeorite impacts was much larger than the present-day value, so that surface regolith was buried before it could build up significant exposure maturity. Models of regolith development on small bodies [*Housen et al.*, 1979; *Hörz and Schaal*, 1981] also suggest that rapid burial from ejecta or spalled material may limit maturity of small body regoliths. As our understanding of the low maturity lunar regolith breccias increases, our ability to interpret meteorite regolith breccias will also increase; the low maturity Apollo 16 regolith breccias are probably the best analogs yet to such meteorites.

SUMMARY

1. The Apollo 16 regolith breccias are extremely low in maturity and are distinct from Apollo 16 soils in maturity, chemistry, and rare gas ratios. This low maturity is largely not an artifact of the breccia-forming process and indicates formation from immature material.

2. $^{40}Ar/^{36}Ar$ ratios for most of these breccias are very high suggesting that the breccias contain very old regolith, perhaps on the order of 4 b.y.

3. These regolith breccias were likely formed in an environment in which large impacts were relatively common. They contain ropy glass and related forms that were likely derived from larger impacts. Agglutinates formed by micrometeorites are very rare.

4. These regolith breccias may have been part of the megaregolith formed during late-stage bombardment of the moon. They may represent lunar regolith developed contemporaneously with the large basin-forming events.

5. The Apollo 16 low maturity regolith breccias may be the best analog in the lunar collection to meteorite regolith breccias.

6. The reason why these primitive regolith breccias dominate at the Apollo 16 site but are rare at Apollo 15, for example, is not clear. Possibly the relatively young South Ray crater at Apollo 16 has caused the recent excavation of large numbers of these breccias from appreciable depths.

APPENDIX 1

The following petrographic descriptions apply to the classification scheme used in the petrographic data tables and figures:

Monomineralic Fragment

Over 90% of a fragment must be a single phase to be considered monomineralic; this guideline was also used by *Houck* [1982].

Anorthosite

Polycrystalline, nearly monomineralic plagioclase with some olivine or pyroxene and rare spinels; using definitions of *Prinz and Keil* [1977], this category includes true anorthosites (>90% plagioclase by visual estimate) and noritic and troctolitic anorthosites (77.5–90% plagioclase). Textures are commonly annealed (granoblastic or poikiloblastic) or cataclastic. Examples shown in *Ryder and Norman* [1980]: cataclastic anorthosite 60015, p. 2, Figure 2*a*; granoblastic anorthosite 60619, p. 133, Figure 2.

Norite-Troctolite

Textures and components like anorthosite, but ferromagnesian minerals are more abundant. This category includes anorthositic norites and troctolites (60–77.5% plagioclase) as well as norites and troctolites (<60% plagioclase) as defined by *Prinz and Keil* [1977]. Example shown in *Ryder and Norman* [1980]: spinel troctolite clast in 67345, p. 827, Figure 2*c*.

KREEP Basalt

Basaltic-textured rock containing significant amounts of SiO_2-rich mesostasis. Example shown in *Ryder and Norman* [1980]: KREEP basalt clast in 67749, p. 979, Figure 2*b*.

Mare Basalt

Basaltic-textured rock lacking significant amounts of SiO_2-rich mesostasis. High titanium basalts are distinguishable by the presence of titaniferous augite and large amounts of ilmenite. Example shown in *Ryder and Norman* [1980]: mare basalt clast in 60639, p. 151, Figure 2*b*.

Regolith Breccia

Fragmental polymict breccia containing agglutinates and/or spherules. Porous and subporous varieties, grouped in "porous" category for modal analyses, have loosely packed matrix (<20 μm) grains. Subcompact and compact breccias, grouped in "compact" category for modal analyses, have less matrix pore space and matrix may even consist of glass in the more highly shocked breccias. Example shown in *Ryder and Norman* [1980]: fragmental polymict breccia 60016, p. 12, Figure 2*a* (porous); dark glassy matrix breccia (regolith breccia?) 60019, p. 35, Figure 2*a* (compact).

Vitric Breccia

Polymict breccia with a glass matrix, which may be devitrified, containing >25% clasts by visual estimate (guideline of *Houck* [1982]); fragments with lower proportions of clasts belong in the clastic/ropy glass category. Example shown in *Ryder and Norman* [1980]: vitric breccia clast in 60016, p. 12, Figure 2*b*.

Fragmental Breccia

Polymict breccia with fragmental to somewhat welded matrix, containing no spherules or agglutinates. Porous textures are like those of porous regolith breccias; compact breccias, with welded matrix-size grains, grade into the vitric breccia category. Example shown in *Ryder and Norman* [1980]: fragmental polymict breccia 67016, p. 783, Figure 2*a* (porous).

Crystalline Matrix Breccia

Fine-grained impact melt with matrix grain sizes generally <50 μm; lithic and mineral clasts of many types may be present. Fine-grained impact melts lacking discernible clasts are also included in this category, however. Even small fragments commonly have a range of matrix textures, so they are classified on the basis of an estimated dominant texture. Examples shown in *Ryder and Norman* [1980]: poikilitic impact melt 65015, p. 558, Figures 2*a* and 2*b* (poikilitic); fine-grained basaltic impact melt 63536, p. 373, Figure 2 (subophitic); variolitic impact melt breccia 60017, p. 21, Figure 2*a* (variolitic).

Clastic/Ropy Glass

Glass with <25% clasts; also ropy glass and glass with schlieren. Examples shown in *Ryder and Norman* [1980]: glass coat on 61535, p. 263, Figure 2; glass coat(?) fragments 65366, p. 628, Figure 2. Many of these particles are self-contained individual glass forms rather than fragments of larger glass objects. Examples are shown in *Fruland et al.* [1977].

Vitrophyric/Quenched Glass

Glass in which all or a large portion has recrystallized; textures include spherulitic, cryptocrystalline, and vitrophyric. Quenched clastic glass is normally classified in this category, also. Examples shown in *Ryder and Norman* [1980]: vesicular glass, white clasts 60665, p. 170, Figure 2*a* (spherulitic); olivine vitrophyre clast in 65095, p. 591, Figure 2*a* (vitrophyre).

Homogeneous Glass

Glass almost or entirely lacking clasts or crystals. Color differentiation may be difficult petrographically due to thin section thickness. Note that black glasses may or may not be of mare origin.

REFERENCES

Ali, M. Z., and W. D. Ehmann, Chemical characterization of lunar core 60009, *Proc. Lunar Sci. Conf. 7th*, 241–258, 1976.

Ali, M. Z., and W. D. Ehmann, Chemical characterization of lunar core 60010, *Proc. Lunar Sci. Conf. 8th*, 2967–2981, 1977.

Bansal, B. M., S. E. Church, P. W. Gast, N. J. Hubbard, J. M. Rhodes, and H. Wiesmann, The chemical composition of soil from the Apollo 16 and Luna 20 sites, *Earth Planet. Sci. Lett., 17*, 29–35, 1972.

Bernatowicz, T. J., C. M. Hohenberg, B. Hudson, B. M. Kennedy, and F. A. Podosek, Excess fission xenon at Apollo 16, *Proc. Lunar Planet. Sci. Conf. 9th*, 1571–1597, 1978.

Bernatowicz, T. J., C. M. Hohenberg, and F. A. Podosek, Xenon component organization in 14301, *Proc. Lunar Planet. Sci. Conf. 10th*, 1587–1616, 1979.

Bernatowicz, T. J., C. M. Hohenberg, B. Hudson, B. M. Kennedy, J. C. Laul, and F. A. Podosek, Noble gas component organization in 14301, *Proc. Lunar Planet. Sci. Conf. 11th*, 629–668, 1980.

Blanchard, D. P., J. W. Jacobs, J. C. Brannon, and R. W. Brown, Drive tube 60009: A chemical study of magnetic separates of size fractions from five strata, *Proc. Lunar Sci. Conf. 7th*, 281–299, 1976.

Bogard, D. D., Chemical abundances and predicted production rates, *Proc. Lunar Planet. Sci. 12B*, 541–558, 1981.

Bogard, D. D., and W. C. Hirsch, Noble gas studies on grain size separates of Apollo 15 and 16 deep drill cores, *Proc. Lunar Sci. Conf. 6th*, 2057–2083, 1975.

Bogard, D. D., and P. Johnson, Trapped noble gases indicate lunar origin for Antarctic meteorite, *Geophys. Res. Lett., 10*, 801–803, 1983.

Fruland, R. M., Regolith Breccia Workbook, Planetary Materials Branch Publ. 66, *JSC 19045*, 269 pp., 1983.

Fruland, R. M., R. V. Morris, D. S. McKay, and U. S. Clanton, Apollo 17 ropy glasses, *Proc. Lunar Sci. Conf. 8th*, 3095–3111, 1977.

Fujii, N., M. Miyamoto, Y. Kobayashi, and K. Ito, Shape of Fe-Ni grains and magnetic susceptibility anisotropy in Antarctic chondrites, *Mem. Natl. Inst. Polar Res. Spec. Issue No.*, 20 pp., 362–371, National Institute of Polar Research, Tokyo, 1981.

Garg, A. N., and W. D. Ehmann, Zr-Hf fractionation in chemically defined lunar rock groups, *Proc. Lunar Sci. Conf. 7th*, 3397–3410, 1976.

Hamano, Y., and K. Yomogida, Magnetic anisotropy and porosity of Antarctic chondrites, *Mem. Natl. Inst. Polar Res., Spec. Issue No. 25*, pp. 281–290, 1982, National Institute of Polar Research, Tokyo, 1982.

Heymann, D., Argon-lead isotopic correlation in samples from lunar maria: records from the ancient lunar regolith, *Earth Planet. Sci. Lett., 27*, 445–448, 1975.

Hörz, F., and R. B. Schaal, Asteroidal agglutinate formation and implications for asteroidal surfaces, *Icarus, 46*, 337–353, 1981.

Houck, K. J., Petrologic variations in Apollo 16 surface soils, *Proc. Lunar Planet. Sci. Conf. 13th*, in *J. Geophys. Res., 87*, A197–A209, 1982.

Housen, K. R., L. L. Wilkening, C. R. Chapman, and G. Greenberg, Asteroidal regoliths, *Icarus, 39*, 317–351, 1979.

James, O. B., Petrologic and age relations of the Apollo 16 rocks: Implications for subsurface geology and the age of the Nectaris Basin, *Proc. Lunar Planet. Sci. 12B*, 209–233, 1981.

James, O. B., and M. K. Florh, Subdivision of the Mg-suite noritic rocks into Mb-gabbronorites and Mg-norites, *Proc. Lunar Planet. Sci. Conf. 13th*, in *J. Geophys. Res., 88*, A603–A614, 1983.

James, O. B., M. K. Flohr, and M. M. Lindstrom, Petrology and geochemistry of lunar dimict breccia 61015, *Proc. Lunar Planet. Sci. Conf. 15th*, in *J. Geophys. Res., 89*, C63–C86, 1984.

Kempa, M. J., J. J. Papike, and C. White, The Apollo 16 regolith: A petrographically constrained mixing model, *Proc. Lunar Planet. Sci. Conf. 11th*, 1341–1355, 1980.

Korotev, R. L., Compositional trends in Apollo 16 soils, *Proc. Lunar Planet. Sci. 12B*, 577–605, 1981.

Korotev, R. L., Comparative geochemistry of Apollo 16 surface soils and samples from cores 64001 and 60002 through 60007, *Proc. Lunar Planet. Sci. Conf. 13th*, in *J. Geophys. Res., 87*, A269–A278, 1982.

Korotev, R. L., Compositional relationships of the pristine nonmare rocks to the highlands soils and breccias, in *Workshop on Pristine Highland Rocks and the Early Evolution of the Moon*, edited by J. Longhi and G. Ryder, pp. 52–55, LPI Tech. Rpt. 83-02, Lunar and Planetary Institute, Houston, 1983.

Korotev, R. L., R. V. Morris, and H. V. Lauer, Jr., Stratigraphy and geochemistry of the Stone Mountain core, *Proc. Lunar Planet. Sci. Conf. 15th*, in *J. Geophys. Res., 89*, C143–C160, 1984.

Korotev, R. L., Geochemical survey of Apollo 15 regolith breccias (abstract), in *Lunar and Planetary Science XVI*, pp. 459–460, Lunar and Planetary Institute, Houston, 1985.

Lakatos, S., and D. Heymann, Green spherules from Apollo 15: inferences about their origin from inert gas measurements, *The Moon*, 132–148, 1973.

Lindstrom, M. M., Alkali gabbronorite, ultra-KREEPy melt rock and the diverse suite of clasts in North Ray Crater, *Proc. Lunar Planet. Sci. Conf. 15th*, in *J. Geophys. Res., 89*, C50–C62, 1984.

Lindstrom, M. M., and D. J. Lindstrom, Lunar granulites and the role of anorthositic norites in the early lunar crust, this volume, 1986.

Lindstrom, M. M., and P. A. Salpas, Geochemical studies of rocks from North Ray Crater, Apollo 16, *Proc. Lunar Planet. Sci. 12B*, B305–B322, 1981.

Lindstrom, M. M., and P. A. Salpas, Geochemical studies of feldspathic fragmental breccias and the nature of North Ray Crater ejecta, *Proc. Lunar Planet. Sci. Conf. 13th*, in *J. Geophys. Res., 88*, A671–A683, 1983.

Lunar Sample Preliminary Examination Team (LSPET), Preliminary examination of lunar samples in *Apollo 16 Preliminary Science Report, NASA SP-315*, pp. 7-1 to 7-58, National Aeronautics and Space Adminstration, Washington, 1972.

Manka, R. H., and F. C. Michel, Lunar atmosphere as a source of argon-40 and other lunar surface elements, *Science, 169*, 278–280, 1970.

MacDougal, D., R. S. Rajan, I. D. Hutcehon, and P. B. Price, Irradiation history and accretionary processes in lunar and meteoritic breccias, *Lunar Sci. Conf. 4th*, 2319–2336, 1972.

McKay, D. S., R. M. Fruland, and G. H. Heiken, Grain size and the evolution of lunar soils, *Proc. Lunar Sci. Conf. 5th*, 887–906, 1974.

McKinley, J. P., G. J. Taylor, K. Keil, M.-S. Ma, and R. A. Schmitt, Apollo 16 impact melt sheets, contrasting nature of the Cayley Plains and Descartes Mountains, and geologic history, *Proc. Lunar Planet. Sci. Conf. 14th*, in *J. Geophys. Res., 89*, B513–B524, 1984.

Megrue, G. H., Spatial distribution of $^{40}Ar/^{39}Ar$ ages in lunar breccia 14301, *J. Geophys. Res., 78*, 3216–3221, 1973.

Minkin, J. A., C. L. Thompson, and E. C. T. Chao, Apollo 16 white boulder consortium samples 67455 and 67475: Petrologic investigation, *Proc. Lunar Sci. Conf. 8th*, 1967–1986, 1977.

Mitchell, J. K., W. N. Houston, R. F. Scott, N. C. Costes, W. D. Carrier, and L. G. Bromwell, Mechanical properties of lunar soil: Density, porosity, cohesion, and angle of internal friction, *Proc. Lunar Sci. Conf. 3rd*, 3235–3253, 1972.

Mizutani, H., and M. Osako, Elastic-wave velocities and thermal diffusivities of Apollo 17 rocks and their geophysical implications, *Proc. Lunar Sci. Conf. 5th*, 2891–2901, 1974.

Morris, R. V., Surface exposure indices of lunar soils: A comparative FMR study, *Proc. Lunar Sci. Conf. 7th*, 315–335, 1976.

Morris, R. V., The surface exposure (maturity) of lunar soils: some concepts and I_s/FeO compilation, *Proc. Lunar Planet. Sci. Conf. 9th*, 2287–2297, 1978.

Morris, R. V., Ferromagnetic resonance and magnetic properties of ALHA81005, *Geophys. Res. Lett., 10*, 807–808, 1983.

Morris, R. V., T. H. See, and F. Hörz, Composition of the Cayley formation at Apollo 16 as inferred from impact melt splashes, this volume, 1986.

Nava, D. F., and J. A. Phillpotts, A lunar differentiation model in light of new chemical data on Luna 20 and Apollo 16 soils, *Geochim. Cosmochim. Acta, 37*, 963–973, 1973.

Oberli, F., J. C. Huneke, and G. J. Wasserburg, U-Pb and K-Ar systematics of cataclysm and precataclysm lunar impactites (abstract), in *Lunar and Planetary Science X*, pp. 940–942, Lunar and Planetary Institute, Houston, 1979.

Pepin, R. O., J. R. Basford, J. C. Dragon, M. R. Coscio, and V. R. Murthy, Rare gases and trace elements in Apollo 15 drill core fines: depositional chronologies and K-Ar ages, and production rates of spallation-produced ^{3}He, ^{21}Ne, and ^{38}Ar versus depth, *Proc. Lunar Sci. Conf. 5th*, 2149–2184, 1974.

Podosek, F. A., and J. C. Huneke, Argon in Apollo 15 green glass spherules (15426): ^{40}Ar-^{39}Ar age and trapped argon, *Earth Planet. Sci. Lett., 19*, 413–421, 1973.

Prinz, M., and K. Keil, Mineralogy, petrology and chemistry of ANT-suite rocks from the lunar highlands, *Phys. Chem. Earth, 10*, 215–237, 1977.

Quaide, W., and T. Bunch, Impact metamorphism of lunar surface materials, *Proc. Apollo 11 Lunar Sci. Conf.*, 711–729, 1970.

Reynolds, J. M., E. C. Alexander, Jr., P. K. Davis, and B. Srinivasan, Studies of K-Ar dating and xenon from extinct radio-activities in breccia 14318: implications for early lunar history, *Geochim. Cosmochim. Acta, 38*, 401–418, 1974.

Russ, G. P., D. S. Burnett, and G. J. Wasserburg, Lunar neutron stratigraphy, *Earth Planet. Sci. Lett., 15*, 172–186, 1972.

Ryder, G., The chemical components of the highlands breccias, *Proc. Lunar Planet. Sci. Conf. 10th*, 561–581, 1979.

Ryder, G., and M. Norman, *Catalog of Apollo 16 Rocks*, Lunar Curatorial Facility Publ. No. 52, 1980.

Schaeffer, G. A., and O. A. Schaeffer, ^{39}Ar-^{40}Ar ages of lunar rocks, *Proc. Lunar Sci. Conf. 8th*, 2253–2300, 1977.

Schultz, L., and H. Kruse, Light noble gases in stony meteorites—a compilation, *Nucl. Track Detect., 2*, 65–103, 1978.

Simkin, T., A. F. Noonan, G. S. Switzer, B. Mason, J. A. Nelen, W. G. Melson, and G. Thompson, Composition of Apollo 16 fines 60051, 60052, 64811, 64812, 67711, 67712, 68821, and 68822, *Proc. Lunar Sci. Conf. 4th*, 279–290, 1973.

Simon, S. B., J. J. Papike, and C. K. Shearer, Petrology of Apollo 11 regolith breccias, *Proc. Lunar Planet. Sci. Conf. 15th*, in *J. Geophys. Res., 89*, C108–C132, 1984.

Spudis, P. D., Apollo 16 site geology and impact melts: Implications for the geologic history of the lunar highlands, *Proc. Lunar Planet. Sci. Conf. 15th*, in *J. Geophys. Res., 89*, C95–C107, 1984.

Stöffler, D., H. -D. Knöll, and U. Maerz, Terrestrial and lunar impact breccias and the classification of lunar highland rocks, *Proc. Lunar Planet. Sci. Conf. 10th*, 639–675, 1979.

Stöffler, D., R. Ostertag, W. U. Reimold, R. Borchardt, J. Malley, and A. Rehfeldt, Distribution and provenance of lunar highland rock types at North Ray Crater, Apollo 16, *Proc. Lunar Planet. Sci. 12B*, 185–207, 1981.

Swindle, T. D., M. W. Caffee, and C. M. Hohenberg, Xenon and other noble gases in shergottites, *Origin of the Moon*, Lunar and Planetary Institute, Houston, in press, 1985.

Takeda, H., H. Mori, M. Miyamoto, and T. Ishii, Mineralogical studies of lunar meteorites and their lunar analogs (abstract), in *Lunar and Planetary Science XVI*, pp. 839–840, Lunar and Planetary Institute, Houston, 1985.

Talwani, M., G. Thompson, B. Dent, H. G. Kable, and S. Buck, Traverse gravimeter experiment, *Apollo 17 Preliminary Science Report, NASA SP-330*, 13-1 to 13-13, 1973.

Taylor, S. R., M. P. Gorton, P. Muir, W. B. Nance, R. Rudowski, and N. Ware, Composition of the Descartes region, lunar highlands, *Geochim. Cosmochim. Acta, 37*, 2665–2685, 1973.

Wänke, H., H. Palme, H. Baddenhausen, G. Dreibus, E. Jagoutz, H. Kruse, B. Spettel, F. Teschke, and R. Thacker, Chemistry of Apollo 16 and 17 samples: Bulk composition, late stage accumulation and early differentiation of the moon, *Proc. Lunar Sci. Conf. 5th*, 1307–1336, 1974.

Wänke, H., H. Palme, H. Baddenhausen, G. Dreibus, E. Jagoutz, H. Kruse, C. Palme, B. Spettel, F. Teschke, and R. Thacker, New data on the chemistry of the lunar samples: Primary matter in the lunar highlands and the bulk composition of the moon, *Proc. Lunar Sci. Conf. 6th*, 1313–1341, 1975.

Wänke, H., H. Baddenhausen, K. Blum, M. Cendales, G. Dreibus, H. Hofmeister, H. Kruse, E. Jagoutz, C. Palme, B. Spettel, R. Thacker, and E. Vilcsek, On the chemistry of lunar samples and achondrites. Primary matter in the lunar highlands: A re-evaluation, *Proc. Lunar Sci. Conf. 8th*, 2191–2215, 1977.

Warren, P. H., and J. T. Wasson, Compositional-petrographic investigation of pristine nonmare rocks, *Proc. Lunar Planet. Sci. Conf. 9th*, 185–217, 1978.

Warren, P. H., and J. T. Wasson, The compositional-petrographic search for pristine nonmare rocks: Third foray, *Proc. Lunar Planet. Sci. Conf. 10th*, 583–610, 1979.

Weber, H. W., and L. Schultz, Rare gases in matrix and clast samples of 60016 (abstract), in *Lunar and Planetary Science IX*, pp. 1234–1236, Lunar and Planetary Institute, Houston, 1978.

Wentworth, S. J., and D. S. McKay, Density and porosity calculations for Apollo 15 and 16 regolith breccias (abstract), in *Lunar and Planetary Science XV*, pp. 906–907, Lunar and Planetary Institute, Houston, 1984.

Yaniv, A., and D. Heymann, Atmospheric ^{40}Ar in lunar fines, *Proc. Lunar Sci. Conf. 3rd*, 1967–1980, 1972.

Yomogida, K., and T. Matsui, Physical properties of some unequilibrated Antarctic ordinary chondrites, *Mem. Natl. Inst. Polar Res. Spec. Issue No. 25*, pp. 281–290, National Institute of Polar Research, Tokyo, 1982.

D. S. McKay, D. D. Bogard, and R. V. Morris, Solar System Exploration Division, Code SN4, NASA Johnson Space Center, Houston, TX 77058.

R. L. Korotev, Department of Earth and Planetary Sciences and the McDonnell Center for the Space Sciences, Washington University, St. Louis, MO 63130.

P. Johnson, Northrop Services, Inc., NASA Johnson Space Center, Houston, TX 77058.

S. J. Wentworth, Lockheed/LEMSCO, NASA Johnson Space Center, Houston, TX 77058.

(Received July 3, 1985;
revised October 29, 1985;
accepted November 18, 1985.)